Tracing the Cambro-Ordovician ferrosilicic to calc-alkaline magmatic association in Iberia by in-situ U–Pb SHRIMP zircon geochronology (Gredos massif, Spanish Central System batholith).

Juan Díaz-Alvarado[a*], Carlos Fernández[b], Martim Chichorro[c], Antonio Castro[d], Manuel Francisco Pereira[e]

[a] *Departamento de Geología, Universidad de Atacama, Copayapu 485, Copiapó, Chile*
[b] *Departamento de Geodinámica y Paleontología, Universidad de Huelva, E-21071 Huelva, Spain*
[c] *CICEGe, Departamento de Ciências da Terra, Universidade Nova de Lisboa, Portugal*
[d] *Unidad Asociada de Petrología Experimental, CSIC-Universidad de Huelva, Campus El Carmen, 21071 Huelva, Spain*
[e] *IDL, Departamento de Geociências, ECT, Universidade de Évora, Portugal*

*Corresponding author
E-mail address: juan.diaza@uda.cl

ABSTRACT

U-Pb geochronological study of zircons from nodular granites and Qtz-diorites comprising part of Variscan high-grade metamorphic complexes in Gredos massif (Spanish Central System batholith) points out the significant presence of Cambro-Ordovician protoliths among the Variscan migmatitic rocks that host the Late Carboniferous intrusive granitoids. Indeed, the studied zone was affected by two contrasted tectono-magmatic episodes, Carboniferous (Variscan) and Cambro-Ordovician. Three main characteristics denote a close relation between the Cambro-Ordovician protholiths of the Prado de las Pozas high-grade metamorphic complex, strongly reworked during the Variscan Orogeny, and other Cambro-Ordovician igneous domains in the Central Iberian Zone of the Iberian Massif: 1) Geochemical features show the ferrosilicic signature of nodular granites. They plot very close to the average analysis of the metavolcanic rocks of the Ollo de Sapo formation (Iberia). Qtz-diorites present typical calc-alkaline signatures and are geochemically similar to intermediate cordilleran granitoids. 2) Both Qtz-diorite and nodular granite samples yield a significant population of Cambro-Ordovician ages, ranging between 483 and 473 Ma, and 487 and 457 Ma respectively. Besides, 3) the abundance of zircon inheritance observed on nodular granites matches the significant component of inheritance reported on Cambro-Ordovician metagranites and metavolcanic rocks of central and NW Iberia.

The spatial and temporal coincidence of both peraluminous and intermediate granitoids, and specifically in nodular granites and Qtz-diorite enclaves of the Prado de las Pozas high-grade complex is conducive to a common petrogenetic context for the formation of both magmatic types. Tectonic and geochemical characteristics describe the activity of a Cambro-Ordovician arc-back-arc tectonic setting associated with the subduction of the Iapetus-Tornquist Ocean and the birth of the Rheic Ocean. The extensional setting is favorable for the generation, emplacement and fast rise of subduction related cold diapirs, supported by the presence of typical calc-alkaline cordilleran granitoids contemporary with ferrosilicic volcanism.

Keywords: Cambro-Ordovician, High-grade metamorphic complexes, Nodular granites, Ferrosilicic magmatism, U–Pb zircon dating, North-Gondwana.

1.- Introduction

The European Variscan Chain resulted from the closure of the Rheic Ocean and the ensuing collision of Gondwana and Laurussia (Matte, 1991; Martínez Catalán et al., 2007, Nance et al., 2010). In NW Iberian Massif, several allochthonous complexes are thrust onto parautochthonous and autochthonous terranes (western part of the European Variscan Chain; e.g., Martínez Catalán et al., 2002). These terranes belong to the North-Gondwana margin (e.g., Martínez Catalán et al., 2002, 2007; Abati et al., 2007; Díez Fernández et al., 2010, 2012a). The pre-Variscan Paleozoic evolution of this tectonic realm includes the formation of a Cambro-Ordovician peri-Gondwanan magmatic arc presumably linked to the subduction of the Iapetus-Tornquist Ocean, and simultaneous opening of the Rheic Ocean triggered by back-arc extension and rifting (e.g., van Staal et al., 1998; Abati et al., 1999, 2007; Winchester et al., 2002; Stampfli and Borel, 2002; Fernández-Suárez et al., 2003; Fuenlabrada et al., 2010; Sánchez Martínez et al., 2012; Díez Fernández et al., 2012b). The analysis of the Cambro-Ordovician magmatism in the Iberian Massif is essential to properly understand the building of the arc and its bearing on the inception of the Rheic Ocean. This widespread magmatism along the northern Gondwana margin comprises rift-related mafic rocks: continental tholeiites (Murphy et al., 2008) and N-MORB, E-MORB and OIB basalts (Sánchez-García et al., 2010), alkaline to peralkaline granites (Pin et al., 1992; Díez Fernández et al., 2012b, 2015), and silicic peraluminous volcanic and plutonic rocks (e.g., Fernández et al., 2008, Díez Montes et al., 2010). These silicic rocks have been associated with the onset of rifting and the formation of migmatites and a core-complex setting in the middle crust (e.g.,

Fernández et al., 2008, Díez Montes et al., 2010). Nevertheless, Cambro-Ordovician magmatism with intermediate composition (60% SiO_2), with a meaningful calc-alkaline signature, is well represented in the Iberian Massif (e.g., Rubio-Ordóñez et al., 2012) in association with voluminous silicic volcanism. This suggests a long-lived subduction active margin prior to and/or during rifting (Díez Montes et al., 2010; Dias da Silva et al., 2014, 2015).

During the past decade, many Variscan metaigneous domains of the Central Iberian Zone (central part of the Iberian Massif) have been ascribed to a late Cambrian to Middle Ordovician (ca. 500-460 Ma) long lasting magmatic event that occurred in North-Gondwana margin (Fig. 1a, Table 1): 1) the so-called "Ollo de Sapo" Formation (Hernández Sampelayo, 1922; Parga Pondal et al., 1964; Martínez Catalán et al., 2004), the best known and most voluminous unit adscribed to Cambro-Ordovician magmatism (Fernández et al., 2008) dated at 495-470 Ma (e.g., Montero et al., 2007, 2009); 2) the pre-Variscan magmatism occurring at the Schist and Greywacke Complex (SGC) Domain, (Valverde and Dunning, 2000; Bea et al., 2003; Zeck et al. 2004), composed mostly of 498-462 Ma metagranites (Montero et al., 2007; Talavera, 2009; Talavera et al., 2013), and 482-470 Ma tonalite–granodiorite igneous bodies to the south (the Beira Baixa-Central Extremadura belt, 482-470 Ma, Antunes et al., 2009; Romão et al., 2010; Rubio-Ordóñez et al., 2012); and 3) the 495-480 Ma volcaniclastic rocks from the Urra Formation and the 493-471 Ma Portalegre granite and Carrascal granite and related gabbros and diorites, in the boundary between the Central Iberian and the Ossa-Morena zones (Solá et al., 2008 and references therein). In addition, a fragment of a Cambro-Ordovician magmatic arc of peri-Gondwanan affinity has been described for the uppermost allochthonous units of the NW Iberian Massif (Abati et al., 1999, 2007; Castiñeiras et al., 2010; Díaz García et al., 2010), and similar associations of Late Ordovician (455±2 Ma) aluminous and metaluminous plutonic rocks, calc-alkaline ignimbrites and epiclastic volcanic rocks have been presented in the northeastern Iberian Peninsula (Álvaro et al., 2008; Murphy et al., 2008; Navidad et al., 2010).

The tectonic scenario drawn by the structural configuration and the geochemical features of Cambro-Ordovician metaigneous domains suggests back-arc extension and rifting in the active continental margin of North-Gondwana (e.g., Arenas et al., 2007; Fernández et al., 2008; Rubio-Ordóñez et al., 2012). Petrogenetically, this back-arc setting, represented by the northern part of the Central Iberian Zone (Ollo de Sapo Domain, Fig. 1a), as well as the basal allochthonous units of NW Iberia (Díez Fernández et al., 2010; Dias da Silva et al., in press), is defined by volcanic belts with high iron and silica contents for very low contents in calcium, crustal isotopic signatures, and a large amount of inherited restitic zircons, interpreted as resulting from a process of almost total melting of subducted sedimentary rocks (fertile material) relaminated in the base of the crust (≈

1000 ° C and 1.5-2 GPa) (Castro et al., 2009, 2013; Talavera, 2009). In turn, the Beira Baixa-Central Extremadura tonalite-granodiorite belt (southern part of the SGC Domain, Fig. 1a) is composed of I-type calc-alkaline intrusive bodies, which suggests that it represents an outward continental magmatic arc relative to the Ollo de Sapo continental back-arc setting (Rubio-Ordóñez et al., 2012). Cambro-Ordovician igneous ages have also been reported for the northern part of the SGC Domain. Orthogneisses (Castilian gneisses, in the sense of Talavera et al., 2013) exposed in the northern part of the Gredos massif, among other places, where recently dated at 498-488 Ma (Talavera et al., 2013).

Coupled petrological–thermomechanical numerical models (Paterson et al., 2011; Vogt et al., 2012) estimate the rates and volumes of magmatic addition expected in active continental margins. The tectonic setting determines the ascent and composition of liquids generated during subduction processes. In extensional settings, the backward motion of the subduction zone leads to necking and rifting processes of the overriding plate. Therefore, large volumes of mafic magmas are formed in the back-arc region (Vogt et al., 2012), whereas the relamination in the crust-mantle or lithosphere-asthenosphere boundary by partially molten cold diapirs, rooted at the subduction channel, possibly determines the formation of an intermediate to felsic magmatic arc (Gerya and Yuen, 2003; Castro and Gerya, 2008; Castro et al., 2010, 2013a; Hacker et al., 2011). Experimental studies carried out in hybrid plumes (subducted sediments and basalts) constrain the conditions and composition of the plume source-for the off-crust generation of intermediate magmas (Castro et al., 2010, 2013b), setting the main characteristics of cordilleran magmatism in active continental margins, which are comparable to those proposed for the origin of ferrosilicic volcanism described in Iberia (Castro et al., 2009).

In the central part of the Gredos massif (Fig. 1b), the genesis of high-grade metamorphic complexes and associated magmatic rocks have been mostly ascribed to Carboniferous processes (Variscan orogeny) despite the limited amount of available radiometric data. In this work, a high-grade metamorphic complex, located in the central part of the Gredos massif (Spanish Central System batholith), is described with the aim of discussing whether or not it represents an older igneous or metamorphic event. U-Pb zircon ages and geochemical features attest an igneous-derived Cambro-Ordovician origin for these Variscan high-grade metamorphic rocks, further expanding the extent and volume of the reported magmatism for this critical tectonic period in the North-Gondwana margin, and pointing possible clues for understanding the close spatial and temporal relationship between the calc-alkaline intermediate and peraluminous silicic magmatism in lower Paleozoic times.

2.- Geological setting

2.1 Ordovician magmatism in the Central Iberian Zone of the Iberian Massif

Early Cambrian to Middle Ordovician igneous and sedimentary rocks, variably metamorphosed during the Variscan cycle (with grade increasing roughly from East to West), together with Variscan granitoids, are well-represented in the Central Iberian Zone of the Iberian Massif. The characterization and interpretation of this magmatism and its tectonic evolution during Cambro-Ordovician times in the North-Gondwana margin have been progressively understood in spite of the extensive Variscan deformation and metamorphism. The Cambro-Ordovician igneous rocks are mainly exposed along three major lineaments: the Ollo de Sapo Domain, the SGC Domain, and the Urra-Portalegre Domain (Fig. 1a).

2.1.1 Ollo de Sapo Domain

The 600 km long Ollo de Sapo Domain includes a variably metamorphosed magmatic association of plutonic, subvolcanic and eruptive facies (Ollo de Sapo Formation) located to the north and central east of the Iberian Massif (Fig. 1a) (Fernández et al., 2008; Montero et al., 2007; Díez Montes et al., 2010). These igneous rocks are characterized by Al saturation index ASI >1, FeO >2.5 wt.%, MgO >0.8 wt.%, for very low contents in calcium (CaO <2.0 wt.%) (Castro et al., 2009) (Table 2, see extended geochemical features in section 4).

The Ollo de Sapo metavolcanic rocks show strong HREE fractionation supporting high-pressure source conditions. Up to 900 °C and 1.0 to 1.1 GPa have been reported for the felsic xenoliths that may represent the lower crust composition in Iberia, and the high-pressure equivalent of Neoproterozoic metagreywackes forming the pre-Variscan basement (SGC Domain) (Villaseca et al., 1999; Fernández et al., 2008). Isotopic compositions of ferrosilicic magmas of the Ollo de Sapo Formation show a narrow variation in Sr–Nd isotopes compared with the Neoproterozoic sediments. $^{87}Sr/^{86}Sr$ initial ratios are between 0.707 and 0.713, and εNd between -5.8 and -3.3 (490-485 Ma) (Fernández et al., 2008; Talavera, 2009). This isotopic signature could be explained by the averaging effect of melting of these heterogeneous protoliths resulting in more homogeneous magmas (Fernández et al., 2008).

The Ollo de Sapo volcanism has been dated between 495±5 and 483±3 Ma (Cambro-Ordovician), followed by an intrusive stage that lasted from 483±3 to 474±4 Ma (Early Ordovician) (Montero et al., 2007) (Table 1). Both meta-effusive and intrusive rocks show an extremelly high proportion (70–80 %) of inherited zircons and zircon cores (Montero et al., 2007; Talavera et al., 2013).

2.1.2 Schist and Greywacke Complex (SGC) Domain: Northern and southern (Beira Baixa-Central Extremadura belt) parts

Parallel to the boundary with the Ollo de Sapo Domain, the northern part of the North SGC Domain contains small Cambro-Ordovician metagranite bodies that are exposed in the Tormes Dome, the Gredos and Guadarrama sectors (Talavera et al., 2013) (Fig. 1a). They are peraluminous and alkali-calcic to calc-alkaline magmas and do not show any significant chemical difference from the rocks of the Ollo de Sapo Formation (Talavera, 2009) (Table 2). Isotopic compositions and geochronological features are identical to those described above for the Ollo de Sapo Formation.

At the southern part of the SGC Domain, the Beira Baixa–Central Extremadura tonalite–granodiorite belt extends for more than 250 km (Fig. 1a). It represents a tonalite–granodiorite calc-alkaline suite intruded in the SGC basement, which resembles a continental magmatic arc (Rubio-Ordoñez et al., 2012). The available U–Pb ages (Antunes et al. 2009; Neiva et al. 2009; Rubio-Ordoñez et al., 2012), obtained from intrusive tonalites and granodiorites, between 482 and 470 Ma (Early Ordovician), are contemporary with the predominantly metaplutonic rocks and volcanic lower Cambrian to Middle Ordovician formations located northwards in the Central Iberian Zone (Table 1).

2.1.3 Urra-Portalegre Domain

The magmatic rocks of the Urra-Portalegre Domain mainly consist of Early Ordovician felsic, porphyritic volcaniclastic rocks. This domain is located in the transition between the Central Iberian and Ossa-Morena zones (SW Iberian Massif) (Fig. 1a) (Solá et al., 2008). Volcanic rocks have rhyolitic to dacitic compositions, are peraluminous and are associated with calc-alkaline granitoids, diorites and gabbros of the same age. $^{87}Sr/^{86}Sr$ initial isotopic signatures range between 0.709 and 0.719, with more restricted εNd (−2.65 to −0.35) (495-470 Ma) (Solá et al., 2008). SHRIMP U-Th-Pb geochronology yields $^{206}Pb/^{238}U$ Cambrian ages ranging from 494.6±6.8 Ma to 488.3±5.2 Ma for the Urra formation (Solá et al., 2008). In this domain, U-Pb ages yield 493-471 Ma (Cambro-Ordovician) for the Portalegre granite, the Carrascal granites and related gabbros and diorites (Solá et al., 2008) (Table 1).

2.2 Gredos massif (Spanish Central System batholith)

The Variscan Spanish Central System batholith (e.g., Moreno-Ventas et al., 1995; Castro et al., 2002), with more than 300 km in length and 60 km in width, provides an almost continuous granite exposure in the Central Iberian Zone (Fig. 1a). Zircon geochronology of granitoids and

mafic igneous rocks of the Spanish Central System batholith and nearby regions yielded an age range of around 320 to 295 Ma, mostly contemporary with or later than the regional, Variscan D3 deformation phase (see age compilation in Díaz-Alvarado et al., 2013). The Gredos massif, located at the central part of the Spanish Central System batholith (Fig. 1b), is composed of granodiorites to monzogranites, which constitute more than 90 vol.% of the intrusive rocks. Minor amounts of gabbro to Qtz-diorite are present in the batholith. In general, all plutonic rocks from gabbros to granodiorites form a typical K-rich, calc-alkaline association (Moreno-Ventas et al., 1995) having close similarities with typical Caledonian I-type batholiths (Chappell and Stephens, 1988), and they belong to the large group of intrusives catalogued as "granodiorites" or "calc-alkaline series granitoids" in regional syntheses and classifications of the Paleozoic magmatism of Iberia (Capdevila et al., 1973; Castro et al., 2002). However, significant differences can be observed among and inside intrusive granitoid bodies, including variable Crd contents and inherited zircons extracted from metasedimentary rocks. These heterogeneities have been interpreted as caused by the interaction (mainly assimilation processes) between the magma and its host rocks (Díaz-Alvarado et al., 2011).

One of the most distinctive features of the Spanish Central System batholith is the presence of upper crustal migmatites with associated anatectic granites (S-type; according to the original definition of Chappell and White, 1974). Metasedimentary rocks occur as large tabular septa, several km in length, and as xenoliths to the scale of a few centimeters to hundreds of meters. Most of these migmatites are derived from pelitic and semipelitic metasedimentary rocks that form part of a several km-thick Neoproterozoic-Cambrian turbiditic series (Rodríguez Alonso et al., 2004).

The metamorphic peak and migmatization in the area occupied by the Spanish Central System batholith took place between 337 and 316 Ma (middle Carboniferous) (e.g., Castiñeiras et al., 2008; Escuder Viruete et al., 1998). PT determinations in the anatectic complexes of the Spanish Central System batholith yielded around 0.4 GPa and 750 °C (middle crust) for the migmatitic conditions (Pereira, 1993; Pereira and Bea, 1994). The general structure of the Spanish Central System batholith in the studied area of the Gredos massif is that of a layered intrusive complex, with distinct magma batches that successively intruded a migmatitic crust (Yenes et al., 1999; Díaz-Alvarado et al., 2013). The emplacement of these tabular magma bodies profited large extensional shear zones affecting the migmatitic host rocks, while U-Pb-Th zircon geochronology of granitoids and mafic igneous rocks of the Spanish Central System batholith and nearby regions reveals that most of the magmatism occurred at 320-295 Ma, as indicated above (e.g., Díaz-Alvarado et al., 2012, 2013; Gutiérrez-Alonso et al., 2011).

Las Pozas high-grade metamorphic complex (Fig. 1b, c) is included in the Gredos massif as a part of the upper and middle crust host-rocks of intrusive late-Variscan granitoids. Nodular granites and nebulites in the central Gredos massif (Fig. 1b, c) define an approximately 5 km in length and 2 km in width elongated, lenticular body limited by the intrusive Variscan granodiorite sheets of Circo de Gredos and Las Pozas, dated at ca. 313 and ca. 304 Ma, respectively (Díaz-Alvarado et al., 2011, 2103). The granitoid sheets show a magmatic foliation defined by the orientation of the preferred orientation of Kfs megacrysts (abbreviations by Kretz, 1983), the parallel arrangement of enclave corridors, schlieren, xenolith septa and igneous leucocratic veins. On the other hand, the metamorphic complex shows a preferred NE-SW orientation defined by sets of restites, nodules, enclaves and leucogranitic lobes, which make a complex nebulitic macrostructure. These sets are present in major contacts between nebulite and nodular granite domains, and may host decimeter-scale shear zones. At the top of the nebulites, nodular granites show magma-magma contacts with intrusive granodiorites (Fig. 1c). A SE-dipping migmatitic folation can be observed in the Las Pozas metamorphic complex, which is sub-parallel to the bulk orientation of the complex and to its external contacts with the intruded granitoid sheets (Fig. 1).

3.- Sampling strategy, field relations and petrography.

3.1 Sampling strategy

Five samples were collected at Prado de las Pozas (Fig. 1c) in order to describe and analyze the geochemical characteristics of the different magmatic and metamorphic rock associations that occur in this high-grade metamorphic complex (Table 2). Due to the close spatial and textural relation between nebulites (J809-10) and nodular granites (J706-43), only the latter were selected for a geochronological study, together with Crd-rich leucogranitic segregates (J809-15) and Qtz-dioritic enclaves (J809-13) (Table 3), in order to clarify their complex intrusive relations.

3.2 Nodular granites and nebulites with Bt-Crd-Sil enclaves

Nodular granites and nebulites with Bt-Crd-Sil enclaves show transitional contacts (although in Fig. 1c they are separated by a continuous layer of Crd-leucgranites) and are mainly melanocratic, heterogeneous rocks (Fig. 2), containing felsic Crd-rich segregates (Fig. 2a), Bt-Crd-Sil restites (Fig. 2b, c) and Kfs nodules (Fig. 2d). Nodular granites are present at the top contact with Las Pozas Bt-granodiorite sheet (Fig. 1c, 2e), where they show abundant Kfs nodules 8-10 cm in diameter (Fig. 2d). Restite alignments, schlierens and other structural markers describe a N30-60E trending

and SE dipping foliation, which is identical to the orientation of the main contacts and to the ductile-brittle shear zones present in nebulites (Fib. 1c). Two distinct nebulite facies constitute most of the high-grade complex (Fig. 1c): a coarse-grained facies, with scarce restites and rich in Kfs nodules; and a medium- to fine-grained facies, rich in restites and leucogranitic segregates (Fig. 2b). Restites, consisting of aggregates of Bt, Crd and Sil, are abundant but heterogeneously distributed (Fig. 2c). Mafic enclaves of quartz-diorite (Fig. 2f), refractory Qtz-nodules and quartzites, and ellipsoidal enclaves of phlebitic migmatite are abundant mostly in nebulites.

Both nebulites and nodular granites consist mainly of anhedral Qtz with undulose extinction, subhedral Bt (Mg#=40-48), subhedral Pl that shows normal zonation with cores of andesine (≈An32) rimmed by an inner band of oligoclase (≈An21) and an outer band of albite (≈An4), subhedral Kfs with perthitic textures, anhedral and subhedral grains of Crd (Mg#=60) and fibrolitic Sil. The main accessory minerals are Ilm, Ap, Tur and Zrn.

3.3 Crd-Leucogranites

Leucocratic granites constitute a continuous sheet at the center of the studied exposure in Prado de las Pozas, central Gredos massif (Fig. 1c) and form lobulate enclaves or lobes within nebulites (Fig. 1c and Fig. 2a). Their most outstanding feature is the presence of abundant, irregularly shaped, Crd cumulates that show a preferred orientation according to the main foliation (Fig. 1c), with no evidence of solid-state structures.

The mineral assemblage consists of rounded Qtz crystals, subhedral grains of Kfs, subhedral Pl grains showing normal zonation (≈An16-3), subhedral grains of Bt (Mg#=36-42) and Crd (Mg#=53-55), which usually contains abundant, small, drop-like inclusions of Qtz. The accessory mineral assemblage consists mainly of Ap and Zrn.

3.4 Mafic rocks

Qtz-dioritic enclaves included within the nebulites (Fig. 2f) and Crd-leucogranites are similar to the mafic microgranular enclaves that are widespread in all types of Carboniferous intrusives in the Gredos massif (e.g., Moreno-Ventas et al., 1995; Bea et al., 1999; Díaz-Alvarado et al., 2011). They are variably sized and shaped, present lobulate contacts with the nebulites, and are commonly clustered in some areas. Moreover, mafic enclaves are also found in leucogranite layers, showing elliptical contour and absence of solid-state fabrics (Fig. 2f).

They are composed of Pl phenocrysts with complex oscillatory zoning (≈An65-32), Qtz and Bt (Mg#=31-40). They also contain domains rich in calcic amphibole as either isolated crystals or polycrystalline aggregates. Accessory minerals are Ilm, Ap and Zrn.

4.- Geochemistry.

Five samples from the high-grade complex of Prado de las Pozas were crushed and milled to very fine powder in steel cups. Whole-rock chemistry of major elements and Zr was analyzed by X-ray fluorescence (XRF) at the University of Oviedo (Spain) using glass beads. Precision of the XRF technique was better than ±1.5% relative. Trace elements, including rare earth elements (REE), were analyzed by inductively coupled plasma mass spectrometry (ICP-MS) with an HP-4500 system at the University of Huelva (Spain), following digestion in an HF + HNO_3 (8:3) solution, drying and further second dissolution in 3 ml HNO_3. The average precision and accuracy for most of the elements were determined by repeated analyses of the SARM-1 (granite) and SARM-4 (norite) international rock standards, and are in the range 5–10% relative.

The results of geochemical analyses are represented in Table 2 and Figure 3. Samples J706-43 (nodular granite), J809-10 (nebulite) and J809-13 (Qtz-diorite) were previously included in a geochemical characterization of the Gredos massif (Díaz-Alvarado et al., 2011).

The composition of the nodular granite is very close to the average analysis of the metavolcanic rocks of the Ollo de Sapo Formation (Iberia). This means a high FeO content in relation to very low CaO (FeO = 3.85 and CaO = 0.87 wt%, Fig. 3a, c, d), moderately peraluminous, Al saturation index ASI = 1.52 (Fig. 3b), and MgO rich (MgO = 1.37 wt.%; Fig. 3c, d). These geochemical features have led some authors to consider them as ferrosilicic rocks (Fernández et al, 2008; Castro et al., 2009). Furthermore, metasedimentary phlebitic enclaves included in the high-grade complexes are geochemically very close to the average composition of Neoproterozoic metagreywackes of the SGC Domain (Table 2), while heterogeneous nebulitic rocks have intermediate characteristics between geochemical signatures of the Ollo de Sapo and SGC domains (Fig. 3).

The Crd-leucogranite is characterized for their exceptionally high FeO contents (FeO = 1.96 wt.%, Table 2) for a high silica (rhyolitic) magma; they are projected very close to the Miranda do Douro and the Antoñita gneisses (Ollo de Sapo Formation) and to the porphyritic volcaniclastic rocks of the Urra formation (Fig. 3c, e).

Instead, Qtz-diorite enclaves belong to the typical calc-alkaline associations of cordilleran granitoids (Fig. 3d, e). No geochemical link between Qtz-diorites and nodular granites or nebulites is observed despite their spatial and temporal relationship.

5.- SHRIMP U-Th-Pb geochronology

340

341 *5.1 Analytical techniques*

342 Zircon separation was carried out at the laboratories of the University of Huelva, using
343 classical procedures including magnetic (Frantz) and density separation. Sample J706-43 (nodular
344 granites) was analyzed with the SHRIMP II (sensitive high resolution ion microprobe) at the
345 Research School of Earth Sciences (Australian National University, Canberra). The non-magnetic,
346 heavy mineral concentration was hand-picked in order to classify and group zircon crystals on the
347 basis of shape, size and lack of fractures or inclusions. The selection of the zircons was random to
348 ensure that all the possible zircon populations are represented. Zircon grains were mounted in epoxy
349 resin together with zircon standards SL13 (U = 238 ppm) and TEMORA ($^{206}Pb/^{238}U$ = 0.06683).
350 The same procedure was carried out for samples J809-13 and J809-15 (Qtz-diorite enclaves and
351 Crd-leucogranite segregates, respectively), which were analyzed in the SHRIMP II instrument at
352 Beijing-SHRIMP Center (Chinese Academy of Geological Sciences, Beijing). The mounts were
353 polished to expose the grain interiors, photographed at high magnification in transmitted and
354 reflected light microscopes and imaged by SEM (scanning electron microscope) (backscattered and
355 cathodoluminescence images) to document the internal growth zoning, inclusions and fractures of
356 the grains. They were then cleaned and coated with high-purity Au in preparation for analysis.
357 Selected areas in zircon grains were analyzed for U, Th and Pb isotopes on both SHRIMP II
358 instruments (RSES: Research School of Earth Sciences, Canberra, and Beijing-SHRIMP Center),
359 using a procedure similar to that described by Williams and Claesson (1987). A 10 kV negative O_2
360 primary beam was focused to ca. 20 μm diameter. Positive secondary ions were extracted at 10 kV
361 and mass analyzed at ca. R5000 mass resolution on a single ETP secondary electron multiplier by
362 peak stepping through the isotopes of interest. Analytical uncertainties are 1σ precision estimates.
363 All the analyses listed and plotted were corrected for common Pb using the measured ^{204}Pb and a
364 common Pb composition appropriate to the age of each spot (Cummings and Richards, 1975).
365 Concordia ages have been calculated with ISOPLOT 3.0 software (Ludwig, 2003). Uncertainties
366 are 95% confidence limits (tσ, where t is the student's t multiplier) and include the uncertainty in the
367 Pb/U calibration (0.3–0.5%).

368

369 *5.2 U-Th-Pb geochronology results*

370 Zircon populations extracted from the nodular granite (J706-43), the Qtz-dioritic enclave
371 (J809-13) and the Crd-leucocratic segregate (J809-15) of the areas studied in this work show a large
372 morphological variety suggesting a complex growth history (Fig. 4). A large amount of inherited
373 crystals and crystal cores has been found (Table 3), and they are interpreted as xenocrysts because

of the crystallization ages and because their zoning is truncated by crystal limits or the overgrowths, respectively. Most of them present uneven overgrowths that yield ages known for major tectono-thermal processes previously described in the Spanish Central System batholith. However, geochronological results also reveal the presence of abundant Cambro-Ordovician ages in the analyzed samples, which had not been described to date in the central part of the Gredos massif.

5.2.1 Sample J809-13. Qtz-dioritic enclaves

Only a few crystals were obtained from Qtz-dioritic enclaves. These grains form a heterogeneous population, variably in size (small- to medium-grained crystals), in morphology (sub-euhedral to sub-rounded, needle-shaped to stubby and equant prisms) and in CL-response (simple acicular zircon with longitudinal zoning, simple concentric oscillatory zoning zircons and composite grains, Fig. 4). Only one analysis, performed on a low-CL unzoned core, has yielded an inherited age of 728 ±16 Ma (Table 3). Four Ordovician ages have been found on acicular and on equant grains, ranging between 483 and 473 Ma (Fig. 5b), yielding a weighted mean age of 480 ±11 Ma (Early Ordovician, 95% conf.; MSWD = 0.18; probability = 0.91), which seems to represent the best estimate of the crystallization age of dioritic melts.

5.2.2 Sample J706-43. Nodular granites

The selected zircons from the nodular granites are complex, heterogeneous crystals, differing in size and morphology (Fig. 4). They show a strong morphological and textural variety. This sample includes acicular simple zircon crystals (e.g., grains 8, 19 and 21 in Figure 4) and subhedral composite grains with inherited cores (e.g., grains 3, 15 and 22; Fig. 4).

The youngest ages are Carboniferous, ranging between 350 and 305 Ma. In addition, the results comprise several groups of inherited ages (lower-middle Proterozoic, Cryogenian-Ediacaran and Cambrian-Ordovician ages). Cambro-Ordovician ages were obtained on a single non-composite acicular grain with oscillatory zoning (21 in Figure 4), with a Th/U ratio of 0.55, on a low-CL unzoned external narrow rim surrounding a polyphase grain (1 in Figure 4), and on a weak concentric zoned intermediate zircon stage (grains 4 and 5 in Figure 4), the last three analyses showing an uniform and a relatively low Th/U ratio (average 0.07). Leaving aside analysis 21 of the single oscillatory zoned crystal, the remaining three analyses are equal within analytical uncertainty (MSWD = 0.21; probability = 0.81), yielding a weighted mean $^{206}Pb/^{238}U$ age of 484.4 ±5.7 Ma (95% conf). This mean age corresponds to the Cambrian-Ordovician transition, and match those obtained on zircons from the Qtz-dioritic enclaves (described above).

Most Carboniferous ages are found in low-CL, unzoned to tenuous concentric zoned overgrowths with very low Th/U ratios (e.g., 9, 18, 22, 25 - Table 3 and Figure 4), consistent with new zircon addition during high-grade metamorphic events (Williams & Claesson 1987; Williams, 1998, Heaman et al. 1990, Wang et al., 2011), spanning a wide range of ages from ca. 350-305 Ma. Also, a needle-shaped non-composite grain with a distinct parallel banded zoning (grain 8, Fig. 4) and a moderate Th/U ratio = 0.8, gave a $^{206}Pb/^{238}U$ age of ca. 323 Ma. The seven Carboniferous ages were concordant within analytical uncertainty, but there was a very large range in their radiogenic 204-corrected $^{206}Pb/^{238}U$ apparent ages. Analysis 11.2 (Table 3) probably overlaps the old detrital host grain, thus giving a Devonian (ca. 397 Ma) apparent age. Two analysis (3.2, 18.1 in Table 3), obtained from overgrowing pyramidal crystal faces, yield 341 and 350 Ma, respectively, and they are equivalent to the oldest ages of migmatization in the Spanish Central System batholith (Peña Negra) (Montero et al., 2004). The remaining $^{206}Pb/^{238}U$ ages span from an upper value of ca. 323 Ma obtained from a layered acicular zircon (grain 8) to a lower end represented by four very low Th/U thin external rims (9, 22, 24 and 25; Table 3) that yielded a late Carboniferous weighted mean $^{206}Pb/^{238}U$ age of 310.6 ±7.4 Ma (95% conf.).

Figure 5a shows the concordia diagram for the nodular granite sample. A detailed section of the diagram (Fig. 5b) highlights the inherited Cambro-Ordovician ages of the nodular granites, together with those of the Qtz-dioritic enclaves and Crd-leucogranites. All Cambro-Ordovician and Carboniferous ages are concordant, suggesting that the youngest ages are not the result of partial radiogenic Pb loss from a primary Ordovician isotopic composition. Rather, the youngest age cluster, together with the Th/U composition in the range 0.01-0.1, represents an independent stage of zircon precipitation during metamorphism or partial melting of a peraluminous rock (Williams & Claesson 1987; Heaman et al. 1990; Williams 2001).

5.2.3 Sample J809-15. Crd-Leucogranites

Leucocratic segregates included in the high-grade complex contain very scarce zircon crystals (low Zr concentration in the whole rock; Table 2). Only 8 zircon crystals were found and CL imaging revealed both composite and simple grains. CL images also show a variable width dark-CL rim surrounding a low or high-CL weakly concentric zoned core in some grains (grains 1, 3 and 4; Fig. 4 and Table 3). Grain 2 is a simple sub-rounded dark-CL unzoned zircon with an excess of Th (very high Th/U ratio), yielding a $^{206}Pb/^{238}U$ age of 280 ±6.8 Ma, equal within analytical uncertainty to analysis 4.1 (287 ±7.4 Ma), obtained from dark-CL unzoned external rim surrounding an internal area through an transgressive interface with evidences of marginal resorption.

Only two analyzed cores yield reliable inherited ages of 512 and 739 Ma. In addition, the younger (Carboniferous) ages (Table 3) match those found in granitoids affected by late U-Th-Pb re-equilibration probably under sub-solidus conditions (Díaz-Alvarado et al., 2013).

6.- Discussion

6.1 Geochemical constraints.

Geochemical features of nodular granites from the Gredos massif match the geochemical signatures of the Cambro-Ordovician ferrosilicic magmatism represented by the Ollo de Sapo Formation and the metavolcanic rocks of the North SGC Domain (Fig. 3). Silica-rich and moderately peraluminous nodular granites (Fig. 3b) show large FeO and MgO contents relative to low CaO values (Fig. 3a, c, d, Table 2). In addition, some of the most prominent textural characteristics in the nodular granites, specifically the presence of K-feldspar nodular megacrysts (Fig. 2d), resemble to those described in the Cambro-Ordovician metavolcanic rocks, in spite of the protracted process of deformation and metamorphism registered in the Gredos massif during the Variscan orogeny (Carboniferous). Moreover, high-grade complexes contain large amounts of enclaves of Qtz-dioritic to tonalitic composition with calc-alkaline affinity (Fig. 3) and Cambro-Ordovician ages (Fig. 4, 5).

Nebulitic migmatites that make up the high-grade metamorphic complexes along with nodular granites show intermediate geochemical features between the SGC Neoproterozoic metasedimentary rocks (found in nebulitic domains as migmatitic enclaves with flebitic textures) and the ferrosilicic rocks (Fig. 3). This is consistent with the complex textural features found in these rocks, where metasedimentary enclaves, K-feldspar nodules and Bt-Crd-Sil restites show chaotic relationships. This suggests that these nebulitic domains are comprised by SGC metasedimentary rocks and ferrosilicic affinity rocks merged together during Variscan tectonic mixing and high-grade metamorphic processes. Leucogranitic dykes and blobs found in nebulites show magma-magma contacts with the nebulite matrix and follow previous rheological weaknesses such as the granite-nebulite boundary. These are high-silica, low CaO and MgO anatectic Crd-leucogranites (Fig. 3d), albeit high FeO contents point to a FeO-rich source like the ferrosilicic rocks. However, according to their Permian zircon ages, the segregation of Crd-leucogranites in the nebulite matrix is probably post-Variscan and not related to the Cambro-Ordovician origin of the ferrosilic igneous protolith.

6.2 The meaning of Cambro-Ordovician and older ages

475 Cambro-Ordovician ages were found in zircons obtained from Qtz-dioritic enclaves and
476 nodular granites located in a high-grade metamorphic complex of the Gredos massif. The Qtz-
477 dioritic enclaves are present as dismembered dyke-like domains (Fig. 1c), forming several blobs of
478 multiple sizes that show complex relations with the host migmatites (both sharp and magma-magma
479 contacts are present in a single enclave, Fig. 2f). The weighted mean $^{206}Pb/^{238}U$ age of 480 ±11 Ma
480 obtained for these intermediate igneous enclaves can be considered equal within analytical
481 uncertainty to the igneous crystallization age obtained for Bercimuelle metagranite located at
482 Northern Gredos (Talavera et al., 2013), as well as similar to those ages obtained from the Urra
483 Formation volcaniclastic rocks ranging from 494.6 ±6.8 Ma to 488.3 ±5.2 Ma (Solá et al., 2008)
484 and localized near the Central Iberian–Ossa-Morena transition zone (SW Iberian Massif) (Fig. 5c,
485 Table 1).
486 Regarding the highly deformed and metamorphosed nebulites and nodular granites, their
487 zircon grains show a strong morphological and textural variety. Textural, morphological,
488 chronological and petrological evidences led to distinguish among zircons crystallized from
489 anatectic melts, zircons removed from paleosomes and zircons from paleosomes overgrown in the
490 anatectic melts (see also Díaz-Alvarado et al., 2011, 2013). The nebulites and nodular granites also
491 provided Cambro-Ordovician ages between 490 and 460 Ma (nodular granite sample, J706-43;
492 Table 3, Fig. 4, 5). These ages are yielded mostly by zircon overgrowths with uniform and
493 relatively low Th/U ratio (average 0.07), although a simple elongated crystal with a Late Ordovician
494 age is present too. These data can be an indication of zircon precipitation from a felsic
495 peraluminous melt (Williams and Claesson 1987; Heaman et al. 1990). Three analyses performed
496 on zircon overgrowths yielded a weighted mean $^{206}Pb/^{238}U$ age of 484.4 ±5.7 (95% conf.), which is
497 essentially equal, within analytical uncertainty, to the age of the Qtz-dioritic enclaves. Therefore,
498 the Cambro-Ordovician ages found in the Qtz-diorite enclaves may indicate that the emplacement
499 of these typical calc-alkaline intrusive rocks approximately coincides with the generation,
500 emplacement and extrusion of ferrosilicic magmatism (Fig. 5).
501 However, Cambro-Ordovician ages represent only 12.5% of the U-Th-Pb ages obtained (32
502 total analyses, Table 3), due to the large number of cores and inherited zircons found in the nodular
503 granite sample. This is consistent with geochronological studies carried out in the Ollo de Sapo
504 formation and other Cambro-Ordovician metavolcanic rocks and gneisses in the Iberian Massif
505 (Montero et al, 2007; Talavera, 2009; Talavera et al., 2013). The high percentage of zircon
506 inheritance observed in nodular granites matches the significant component of inheritance reported
507 on Cambro-Ordovician metagranites and metavolcanic rocks of central and NW Iberia composed of
508 Ediacaran–Early Cambrian (65%) and, to a lesser extent, Cryogenian, Tonian, Mesoproterozoic,

Orosirian and Archean pre-magmatic cores (Fig. 6) (Montero et al, 2007; Talavera, 2009; Talavera et al., 2013). The Ollo de Sapo and Urra Formations show a simple Ediacaran population (600-610 Ma), whereas the NW Iberian and Central Iberian orthogneisses exhibit three populations at 540-550, 575-585 and 605-615 Ma (Talavera et al., 2013). The studied nodular granites yielded two Ediacaran populations at ca. 570 and 620 Ma (Fig. 6a). Moreover, they show an outstanding frequency of young Cryogenian ages (640-660 Ma), as well as the absence of Mesoproterozoic (Stenian) zircons. These features make them slightly different from those observed in other Cambro-Ordovician igneous rocks of the Iberian Massif. A compilation of U-Pb ages from inherited zircon grains analyzed on Cambro-Ordovician metagranites and metavolcanic rocks from other sections of the Western European Variscan Belt performed by Talavera et al. (2013) shows three distinctive Ediacaran-Early Cambrian populations whose statistical age ranges match those of the Iberian Cambro-Ordovician rocks, including those obtained in this work. Therefore, despite local heterogeneities, the source that has undergone partial melting to give this Cambro-Ordovician magmatism is essentially Pan-African (e.g. Talavera et al., 2013) and/or Cadomian (Pereira, 2014).

Although the number of analysis providing pre-Ordovician ages (inherited cores and zircons) does not allow us to be conclusive and the geochronological data must be taken cautiously, the comparison of these results with those obtained in the main igneous and sedimentary units ascribed to the Ordovician period could shed light on the complex origin of nodular granites and associated nebulites from the Gredos massif (Fig. 6b, c). In this sense, the high frequency of early Ediacaran-late Cryogenian ages (620-660 Ma) in nodular granites is characteristic of Central Iberian gneisses in contrast to NW Iberian gneisses (Fig. 6c). These ages and the marginal representativity of Mesoproterozoic (Stenian) zircons bear striking similarities with the late Ediacaran SGC (Beiras Group) and with the Early Ordovician arkosic quartzite of the Sarnelhas Formation from the southwest Central Iberian Zone (Pereira et al., 2012) (Fig. 6b). In particular, the affinities with Sarnelhas arkosic quartzite are remarkable because this unit is characterized by a significant population of Ediacaran-Cryogenian detrital zircons and only a few Tonian and Mesoproterozoic ages (percentages <1%).

6.3 The meaning of late Paleozoic ages.

The youngest zircon ages (7 analyses) yielded by the nodular granite sample (J706-43; Table 3) point to a protracted metamorphic record during Carboniferous times, in addition to a Cambro-Ordovician magmatic event. These ages were found by analyzing thin overgrowths over rounded inherited zircons of different ages, except for grain 8 (Fig. 4). Furthermore, these analyses mostly have Th/U ratio less than 0.01, which is usually related to metamorphic processes (Wang et al.,

2011). The Carboniferous ages found in these overgrowths can be grouped in two main events: 1) two ages of 350-340 Ma account for the older Variscan migmatization events (Montero et al., 2004), and 2) five ages (323-305 Ma) are contemporary to the intrusive phase during the batholith building (Díaz-Alvarado et al., 2013). This wide range of ages reflects that the high-grade (essentially high-temperature) conditions were maintained during a continuous emplacement and amalgamation of a number of intrusive granitoid layers that comprise the batholith (Díaz-Alvarado et al., 2013).

Early Permian ages found in the leucogranitic segregates (J809-15; Table 3) included in the nebulites have been described in the intrusive granitoids (Díaz-Alvarado et al., 2013) and, though secondary processes are not discarded (Pb loss or deformation along sub-solid shear zones may affect the isotopic ratios), they point out that the complex texture, internal structure and lithological variety of nebulites are due to the superposition of high-grade metamorphic and anatectic processes that may reach the Permian. Nevertheless, concordant data would not exclude the possibility that only the younger group represents a real igneous-metamorphic event, and that isotopic disequilibrium has left a trail of meaningless ages (Bea and Montero, 2013).

6.4 Tectonic setting.

The extensive Cambro-Ordovician ferrosilicic intrusive granitoids and their sub-volcanic and extrusive counterparts evidence the close relationship between ferrosilicic and calc-alkaline magmatism during the Cambro-Ordovician magmatic event found in the Central Iberian Zone and the Galicia-Trás-os-Montes Zone: (i) Ollo de Sapo Domain near the contact between the Central Iberian and West-Asturian Leonese zones; (ii) Northern SGC Domain defined by the lineament of the Central Iberian and NW Iberian orthogneisses; iii) Beira Baixa-Central Extremadura tonalite-granodiorite belt that extends from Gouveia (Portugal) to Zarza (Spain); iv) Portalegre-Urra domain at the Central Iberian–Ossa-Morena transition zone (SW Iberian Massif) (Table 1). Indeed, recently, it has been proposed the presence of a Cambro-Ordovician magmatic arc in the Central-Iberian Zone (the Beira Baixa-Central Extremadura belt) (Rubio-Ordóñez et al., 2012; Díez Fernández et al., 2015). Qtz-dioritic enclaves found in the Gredos massif (Prado de las Pozas), which plot into the calc-alkaline series of cordilleran magmatism, may represent evidence of the existence of such Cambro-Ordovician magmatic arc.

Figure 7 shows a schematic section of the northern Gondwana margin during Cambro-Ordovician times based on previous works (Fernández et al., 2008; Rubio Ordóñez et al., 2012; Villaseca et al., 2014) and new geochemical and geochronological data from high-grade complexes of the Gredos massif. The coincidence of subduction processes and an extensional setting in the

back-arc region promoted the concurrency of calc-alkaline magmatism, typical of active continental margins, and the generation of peraluminous ferrosilicic magmas related to the emplacement of sedimentary material (cold diapirs) in the lithosphere mantle. This Cambro-Ordovician magmatic event has been described in the realm of a back-arc rifting that affected the active continental margin of North-Gondwana during the inception of the Rheic Ocean (e.g., van Staal et al., 1998; Stampfli and Borel, 2002; Fuenlabrada et al., 2010; Díez Fernández et al., 2012b). The extensional tectonic setting within the active continental margin is favorable for the generation of cold diapirs, mainly formed by sedimentary material introduced into the subduction channel (Fernández et al., 2008; Castro et al., 2009). This extensional setting allows the emplacement (relamination in the sense of Hacker et al., 2011) of these cold diapirs at the top of the mantle wedge and facilitates their fast rise throughout the crust. The high pressures and temperatures estimated to generate the ferrosilicic magmatism and the large concentration of inherited ages point to a process of high-percentage melting in the crust-mantle boundary and a rapid ascent to shallow depths in the crust to generate ferrosilicic magmatism. Silicic compositions ("cold granites", in the sense of Miller et al., 2003), and the brief time for zirconium dissolution processes could explain these anomalous abundances in inherited zircons. The presence of typical calc-alkaline cordilleran granitoids contemporary with ferrosililicic volcanism supports a subduction-related origin for the Cambro-Ordovician magmatism asserted on the generation of hybrid-andesitic plumes.

7.- Conclusions

Nodular granites and nebulites from the Gredos massif constitute an important domain in the high-grade metamorphic complexes present as part of the middle crust that host late Paleozoic granitoids in the Spanish Central System batholith. These rocks are closely related to Neoproterozoic metasedimentary rocks that constitute the SGC, and have been highly deformed and metamorphosed (nebulitic textures depict a large partial melting percentage) in the course of the Variscan orogeny.

Geochemically, nodular granites are rich in silica, moderately peraluminous and rich in FeO and MgO relative to the low CaO. These geochemical features clearly relate these rocks to crustal sources that include the ferrosilicic Cambro-Ordovician magmatism of the Ollo de Sapo, north of SGC and Urra-Portalegre domains. Qtz-diorite enclaves are present within these high-grade complexes (nebulitic migmatites, nodular granites and Crd-leucogranites). They show calc-alkaline geochemical signatures and complex textural relations with the host migmatites. Cambro-Ordovician ages (between 490 and 460 Ma) found in nodular granites and Qtz-diorite enclaves of

the Gredos massif confirm that these high-grade complexes are in part derived from igneous-sedimentary complexes related to the extensive Cambro-Ordovician magmatic event that affected the North-Gondwana margin.

The narrow spatial and temporal link between the peraluminous ferrosilicic and the cordilleran calc-alkaline magmatism points to the evolution of a magmatic arc associated with the subduction of the Iapetus or Tornquist Ocean, and to the activity of an arc-back-arc tectonic setting during the the inception of the Rheic Ocean. The details of this process are not fully understood, although the presence and interaction of contemporary ferrosilic and calc-alkaline magmatic rocks in the central part of the Gredos massif should be taken into account and adequately explained in future models of the Cambro-Ordovician evolution of the North-Gondwana margin.

Although ferrosilic and calc-alkaline magmatism have been located in very specific and separated tectonic settings on the structural configuration of the Cambro-Ordovician northern margin of Gondwana, the coalescence of intrusive Qtz-diorites and ferrosilicic nodular granites in intermediate areas points to similar petrogenetic conditions for this magmatic association, as has already been proved by experimental petrology. The generation of hybrid-andesitic plumes and cold diapirs of sedimentary material, and their relamination in the crust-mantle boundary is a feasible explanation for the extensive magmatism that accompanies the opening of the Rheic Ocean during the Cambro-Ordocian evolution of the North-Gondwana margin.

Acknowledgments

Part of this work was developed during the PhD Thesis of J.D.A., carried out at the Departments of Geology and Geodynamics and Paleontology, University of Huelva, with a Grant Fellowship from the Spanish Ministry of Science and Innovation (grant no. AP2005-3498). The work was funded with Projects CGL2004-06808-CO4-01/BTE, CGL2004-06808-CO4-02/BTE, CGL2007-63237/BTE, and CGL2010-22022-CO2-01 of the Spanish Ministry of Science and Innovation, and supported by the Project DIUDA-22268 of the University of Atacama. This work pays tribute to and relies on the tireless activity of Cecilio Quesada to help to unravel the intricacies of the Variscan and pre-Variscan tectonic evolution of Iberia. Richard Armstrong assisted for the technical support with SHRIMP work at ANU (Canberra) and Xie Hangqiang at SHRIMP Beijing Center (China). We would like to sincerely thank the editor and the reviewers (Rubén Díez Fernández and others) of Tectonophysics for their thorough corrections of the first draft of this manuscript.

References

Abati, J., Dunning, G.R., Arenas, R., Díaz García, F., González Cuadra, P., Martínez Catalán, J.R., 1999. Early Ordovician orogenic event in Galicia (NW Spain): evidence from U–Pb ages in the uppermost unit of the Ordenes Complex. Earth and Planetary Science Letters 165, 213–228.

Abati, J., Castiñeiras, P., Arenas, R., Fernández-Suárez, J., Gómez Barreiro, J., Wooden, J.L., 2007. Using SHRIMP zircon dating to unravel tectonothermal events in arc environments. The early Paleozoic arc of NW Iberia revisited. Terra Nova 19, 432-439.

Álvaro, J.J., Ezzouhairi, H., Ribeiro, M.L., Ramos, J.F., & Solá, A.R., 2008. Early Ordovician volcanism in the Iberian Chains (NE Spain) and its influence on the preservation of shell concentrations. Bull. Soc. géol. Fr. 6, 569-581.

Antunes, I.M.H.R., Neiva, A.M.R., Silva, M.M.V.G. & Corfu, F., 2009. The genesis of I- and S-type granitoid rocks of the Early Ordovician Oledo pluton, Central Iberian Zone (central Portugal). Lithos 111, 168–85.

Arenas, R., Martínez Catalán, J.R., Sánchez Martínez, S., Fernández- Suárez, J., Andonaegui, P., Pearce, J.A., Corfu, F., 2007. The Vila de Cruces ophiolite: A remnant of the early Rheic Ocean in the Variscan suture of Galicia (northwest Iberian Massif). The Journal of Geology 115, 129-148.

Bea, F., Montero, P., Molina, J. F., 1999. Mafic precursors, peraluminous granitoids, and late lamprophyres in the Avila batholith: A model for the generation of Variscan batholiths in Iberia. Journal of Geology 107, 399-419.

Bea, F., Montero, P., Zinger, T., 2003. The nature, origin, and thermal influence of the granite source layer of Central Iberia. The Journal of Geology 111, 579–595.

Bea, F., Villaseca, C., Bellido, F., 2004. El Batolito de Ávila (Sistema Central Español). In: Vera, J.A. (Ed.), Geología de España. SGE-IGME, Madrid, pp. 101–110.

679 Bea, F., Montero, P., Talavera, C., Zinger, T., 2006. A revised Ordovician age for the oldest
680 magmatism of Central Iberia: U-Pb ion microprobe and LA-ICPMS dating of the Miranda
681 do Douro orthogneiss. Geol. Acta 4, 395–401.
682
683 Bea, F., Montero, P., 2013. Diffusion-induced disturbances of the U–Pb isotope system in pre-
684 magmatic zircon and their influence on SIMS dating. A numerical study. Chemical Geology
685 349–350, 1–17.
686
687 Beetsma, J.J., 1995. The late Proterozoic/Paleozoic and Hercynian crystal evolution of the Iberian
688 Massif, N Portugal. Ph.D. Thesis, Vrije University, Amsterdam, 223 pp.
689
690 Briggs, W.D., 1995. Pressure–temperature-deformation history of the Ollo de Sapo Antiform,
691 Variscan Orogen, Northwest Spain. Ph.D. thesis, University of Cincinnati.
692
693 Capdevila, R., 1969. Le metamorphisme regional progressif et les granites dans le segment
694 Hercynien de Galice Nord Orientale (NW de L'Espagne). Ph.D. thesis, University of
695 Montpellier.
696
697 Capdevila, R., Corretgé, L. G., Floor, P., 1973. Les granitoides varisques de la Mesete Iberique.
698 Bulletin de la Société Géologique de France 15, 209-228.
699
700 Castiñeiras, P., Villaseca, C., Barbero, L., Martín Romera, C., 2008. SHRIMP U–Pb zircon dating
701 of anatexis in high-grade migmatite complexes of central Spain: implications in the
702 Hercynian evolution of Central Iberia. International Journal of Earth Sciences 97, 35–50.
703
704 Castiñeiras, P., Díaz García, F., Gómez Barreiro, J., 2010. REE-assisted U–Pb zircon age
705 (SHRIMP) of an anatectic granodiorite: Constraints on the evolution of the A Silva
706 granodiorite, Iberian allochthonous complexes. Lithos 116, 153–166.
707
708 Castro, A., Corretgé, L.G., El-Biad, M., El-Hmidi, H., Fernández, C., Patiño-Douce, A.E., 2000.
709 Experimental constraints on Hercynian Anatexis in the Iberian Massif, Spain. Journal of
710 Petrology 41, 1471–1488.
711

712 Castro, A., Corretgé, L. G., De La Rosa, J., Enrique, P., Martínez, F. J., Pascual, E., Lago, M.,
713 Arranz, E., Galé, C., Fernández, C., Donaire, T., López, S., 2002. Paleozoic magmatism. In:
714 Gibbons, W. & Moreno, M. T. (eds) The Geology of Spain. London: Geological Society, pp.
715 117-153.
716
717 Castro, A., Corretgé, L.G., de la Rosa, J.D., Fernández, C., López, S., García-Moreno, O., Chacón,
718 H., 2003. The appinite–migmatite complex of Sanabria, NW Iberian Massif, Spain. Journal
719 of Petrology 44 (7), 1309–1344.
720
721 Castro, A., Gerya, T.V., 2008. Magmatic implications of mantle wedge plumes: experimental study.
722 Lithos 103, 138–148.
723
724 Castro, A., García-Casco, A., Fernández C., Corretgé L.G., Moreno-Ventas I., Gerya T., Löw, I.,
725 2009. Ordovician ferrosilicic magmas: Experimental evidence for ultrahigh temperatures
726 affecting a metagreywacke source. Gondwana Research 16, 622–632.
727
728 Castro, A., Gerya, T., García-Casco, A., Fernández, C., Díaz Alvarado, J., Moreno-Ventas, I.,
729 Loew, I., 2010. Melting relations of MORB-sediment mélanges in underplated mantle
730 wedge plumes. Implications for the origin of cordilleran-type batholiths. Journal of
731 Petrology 51, 1267–1295.
732
733 Castro, A., Vogt, K., Gerya, T., 2013a. Generation of new continental crust by sublithospheric
734 silicic-magma relamination in arcs: A test of Taylor's andesite model. Gondwana Research
735 23, 1554–1566.
736
737 Castro, A., 2013b. Tonalite–granodiorite suites as cotectic systems: A review of experimental
738 studies with applications to granitoid petrogenesis. Earth-Science Reviews 124, 68–95.
739
740 Chappell, B. W., Stephens, W. E., 1988. Origin of infracrustal (I-type) granite magmas.
741 Transactions of the Royal Society of Edinburgh, Earth Sciences 79, 71-86.
742
743 Chappell, B.W., White, A.J.R., 1974. Two contrasting granite types. Pacific Geology 8, 173–174.
744

745 Corretgé, L.G., Castro, A., El-Hmidi, H., García-Moreno, O., 2001. Characteristics and significance
746 of the experimental products from partial melting of rocks from the "Complejo Esquisto
747 Grauváquico" at 3.5 kbar. Abstracts Congreso Ibérico de Geoquímica, Zaragoza, Instituto
748 Tecnológico de Aragón, pp. 191–196.
749
750 Cummings, G.L., Richards, J.R., 1975. Ore lead isotope ratios in a continuously changing Earth.
751 Earth and Planetary Science Letters 28, 155–171.
752
753 Debon, F., Le Fort, P., 1983. A chemical–mineralogical classification of common plutonic rocks
754 and associations. Transactions of the Royal Society of Edinburgh: Earth Sciences 73, 135–
755 149.
756
757 Debon, F., Le Fort, P., 1988. A cationic classification of common plutonic rocks and their magmatic
758 association: principles, method, application. Bulletin de Minéralogie 111, 493–510.
759
760 Dias da Silva, Í., Valverde-Vaquero, P., González-Clavijo, E., Díez-Montes, A., Martínez Catalán,
761 J.R., 2014. Structural and stratigraphical significance of U–Pb ages from the Mora and
762 Saldanha volcanic complexes (NE Portugal, Iberian Variscides). Geological Society,
763 London, Special Publications 405, 115-135.
764
765 Dias da Silva, Í., Díez Fernández, R., Díez-Montes, A., González-Clavijo, E., Foster, D.A., 2015.
766 Magmatic evolution in the N-Gondwana margin related to the opening of the Rheic Ocean:
767 evidence from the Upper Parautochthon of the Galicia-Trás-os-Montes Zone and from the
768 Central Iberian Zone (NW Iberian Massif). International Journal of Earth Sciences, doi:
769 10.1007/s00531-015-1232-9.
770
771 Díaz-Alvarado, J., Castro, A., Fernández, C., Moreno-Ventas, I., 2011. Assessing bulk assimilation
772 in cordierite-bearing granitoids from the Central System batholith, Spain; experimental,
773 geochemical and geochronological constraints. Journal of Petrology 52, 223–256.
774 doi:10.1093/petrology/egq078
775
776 Díaz-Alvarado, J., Fernández, C., Díaz Azpiroz, M., Castro, A., Moreno-Ventas, I., 2012. Fabric
777 evidence for granodiorite emplacement with extensional shear zones in the Variscan Gredos

778 massif (Spanish Central System). Journal of Structural Geology 42, 74–90.
779 http://dx.doi.org/10.1016/j.jsg.2012.06.012
780
781 Díaz-Alvarado, J., Castro, A., Fernández, C., Moreno-Ventas, I., 2013. SHRIMP U–Pb zircon
782 geochronology and thermal modeling of multilayer granitoid intrusions. Implications for the
783 building and thermal evolution of the Central System batholith, Iberian Massif, Spain.
784 Lithos 175–176, 104–123. http://dx.doi.org/10.1016/j.lithos.2013.05.006
785
786 Díaz García, F., Sánchez Martínez, S., Castiñeiras, P., Fuenlabrada, J.M., Arenas, R., 2010. A peri-
787 Gondwanan arc in NW Iberia. II: Assessment of the intra-arc tectonothermal evolution
788 through U–Pb SHRIMP dating of mafic dykes. Gondwana Research 17, 352-362.
789
790 Díez Fernández, R., Martínez Catalán, J.R., Gerdes, A., Abati, J., Arenas, R., Fernández-Suárez, J.,
791 2010. U-Pb ages of detrital zircons from the Basal allochthonous units of NW Iberia:
792 Provenance and paleoposition on the northern margin of Gondwana during the
793 Neoproterozoic and Paleozoic. Gondwana Research 18, 385-399.
794
795 Díez Fernández, R., Martínez Catalán, J.R., Arenas, R., Abati, J., 2012a. The onset of the assembly
796 of Pangaea in NW Iberia: Constraints on the kinematics of continental subduction.
797 Gondwana Research 22, 20-25.
798
799 Díez Fernández, R., Castiñeiras, P., Gómez-Barreiro, J., 2012b. Age constraints on Lower Paleozoic
800 convection system: Magmatic events in the NW Iberian Gondwana margin. Gondwana
801 Research 21, 1066-1079.
802
803 Díez Fernández, R., Pereira, M.F., Foster, D.A., 2015. Peralkaline and alkaline magmatism of the
804 Ossa-Morena zone (SW Iberia): Age, source, and implications for the Paleozoic evolution of
805 Gondwanan lithosphere. Lithosphere 7, 73-92.
806
807 Díez Montes, A., Martínez Catalán, J.R., Bellido Mulas, F., 2010. Role of the Ollo de Sapo massive
808 felsic volcanism of NW Iberia in the early ordovician dynamics of northern Gondwana.
809 Gondwana Research 17, 363–376.
810

811 Escuder Viruete, J., Hernáiz Huerta, P.P., Valverde-Vaquero, P., Rodríguez Fernández, R.,
812 Dunning, G., 1998. Variscan syncollisional extension in the Iberian Massif: structural,
813 metamorphic and geochronological evidence from the Somosierra sector of the Sierra de
814 Guadarrama (Central Iberian Zone, Spain). Tectonophysics 290, 87–109.
815
816 Farias, P., Ordóñez-Casado, B., Marcos, A., Robio-Ordóñez, A., Fanning, C.M., 2014. U–Pb zircon
817 SHRIMP evidence for Cambrian volcanism in the Schistose Domain within the Galicia-
818 Trás-os-Montes Zone (Variscan Orogen, NW Iberian Peninsula). Geol. Acta 12, 209–218.
819
820 Fernández, C., Becchio, R., Castro, A., Viramonte, J. M., Moreno-Ventas, I., Corretgé, L. G., 2008.
821 Massive generation of atypical ferrosilicic magmas along the Gondwana active margin:
822 Implications for cold plumes and back-arc magma generation. Gondwana Research 14, 451-
823 473.
824
825 Fernández-Suárez, J., Díaz García, F., Jeffries, T.E., Arenas, R., Abati, J., 2003. Constraints on the
826 provenance of the uppermost allochthonous terrane of the NW Iberian Massif: inferences
827 from detrital zircon U–Pb ages. Terra Nova 15, 138–144.
828
829 Fuenlabrada, J.M., Arenas, R., Sánchez Martínez, S., Díaz García, F., Castiñeiras, P., 2010. A peri-
830 Gondwanan arc in NW Iberia. I: Isotopic and geochemical constraints on the origin of the
831 arc- A sedimentary approach. Gondwana Research 17, 338-351.
832
833 García de Figuerola, L.G., 1966. Datos petrológicos de la Sierra de Gata (Cáceres). Revista de la
834 Facultad de Ciencias, Universidad de Salamanca 7 (1), 53–80.
835
836 Gerya, T.V., Yuen, D.A., 2003. Rayleigh–Taylor instabilities from hydration and melting propel
837 'cold plumes' at subduction zones. Earth and Planetary Science Letters 212, 47–62.
838
839 Gil Ibarguchi, J.I., 1978. Etude petrographique de la region Muxia-Finisterre (NW de L'Espagne).
840 Ph.D. thesis, University of Paris VI.
841
842 Gutiérrez-Alonso, G., Fernández Suárez, J., Jeffries, T.E., Johnston, S.T., Pasto-Galán, D., Murphy,
843 J.B., Franco, M.P., Gonzalo, J.C., 2011. Diachronous post-orogenic magmatism within a

developing orocline in Iberia, European Variscides. Tectonics 30, TC5008. http://dx.doi.org/10.1029/2010TC002845.

Gutiérrez-Alonso, G., Gutiérrez-Marco, J.C., Fernández-Suárez, J., Bernárdez, E., Corfu, F., 2016. Was there a super-eruption on the Gondwanan coast 477Ma ago?. Tectonophysics, http://dx.doi.org/10.1016/j.tecto.2015.12.012

Hacker, B.R., Kelemen, P.B., Behn, M.D., 2011. Differentiation of the continental crust by relamination. Earth and Planetary Science Letters 307, 501-516.

Heaman, L.M., Bowins, R., Crocket, J., 1990. The chemical composition of igneous zircon studies: implications for geochemical tracer studies. Geochimica et Cosmochimica Acta, 54, 1597–1607.

Hernández Sampelayo, P., 1922. Hierros de Galicia. Memorias Instituto Geológico y Minero de España, Madrid 466 pp.

Holtz, F., 1987. Etude structurale, métamorphique et geochimique des granitoides Hercyniens et de leur encaissant dans la region de Montalegre. Ph.D. thesis, University of Nancy.

Kretz, R., 1983. Symbols for rock-forming minerals. American Mineralogist, 68, 277-279.

Ludwig, K.R., 2003. Isoplot 3.0 a geochronological toolkit for Microsoft Excel. Special Publication No. 4. Berkeley Geochronology Center, Berkeley, California 71 pp.

Martínez Catalán, J.R., Díaz García, F., Arenas, R., Abati, J., Castiñeiras, P., González Cuadra, P., Gómez Barreiro, J., Rubio Pascual, F., 2002. Thrust and detachment systems in the Órdenes Complex (northwestern Spain): implications for the Variscan–Appalachian geodynamics. In: Martínez Catalán, J.R., Hatcher Jr., R.D., Arenas, R., Díaz García, F. (Eds.), Variscan-Appalachian Dynamics: the building of the Late Paleozoic Basement: Geological Society of America Special Paper, vol. 364, pp. 163–182.

876 Martínez Catalán, J.R., González Lodeiro, F., González Clavijo, E., Fernández, C., Díez Montes,
877 A., 2004. Dominio del Ollo de Sapo: estructura. In: Vera, J.A. (Ed.), Geología de España,
878 SGE-IGME, Madrid, pp. 75–78.
879
880 Martínez Catalán, J.R., Arenas, R., Díaz García, F., González Cuadra, P., Gómez-Barreiro, J.,
881 Abati, J., Castiñeiras, P., Fernández-Suárez, J., Sánchez Martínez, S., Andonaegui, P.,
882 González Clavijo, E., Díez Montes, A., Rubio Pascual, F.J., Valle Aguado, B., 2007. Space
883 and time in the tectonic evolution of the northwestern Iberian Massif: implications for the
884 Variscan belt. In: Hatcher Jr., R.D., Carlson, M.P., McBride, J.H., Martínez Catalán, J.R.
885 (Eds.), 4-D Framework of Continental Crust: Geological Society of America Memoir, vol.
886 200, pp. 403–423.
887
888 Matte, Ph., 1991. Accretionary history and crustal evolution of the Variscan belt in Western Europe.
889 Tectonophysics 196, 309–337.
890
891 Miller, C.F., McDowell, S.M., Mapes, R.W., 2003. Hot and cold granites? Implications of zircon
892 saturation temperatures and preservation of inheritance. Geology 31, 529–532.
893
894 Montero, P., Bea, F., Zinger, T.F., Scarrow, J.H., Molina, J.F., Whitehouse, M., 2004. 55 million
895 years of continuous antexis in Central Iberia: single-zircon dating of the Peña Negra
896 Complex. Journal of the Geological Society of London 161, 255–263.
897
898 Montero, P., Bea, F., González-Lodeiro, F., Talavera, C., Whitehouse, M.J., 2007. Zircon ages of
899 the metavolcanic rocks and metagranites of the Ollo de Sapo Domain in central Spain:
900 implications for the Neoproterozoic to Early Palaeozoic evolution of Iberia. Geological
901 Magazine 144, 963–76.
902
903 Montero, M.P., Talavera, C., Bea, F., González Lodeiro, F., Whitehouse, M.J., 2009. Zircon
904 geochronology of the Ollo de Sapo Formation and the age of the Cambro-Ordovician rifting
905 in Iberia. Journal of Geology 117, 174–191.
906
907 Moreno-Ventas, I., Rogers, G., Castro, A., 1995. The role of hybridization in the genesis of
908 Hercynian granitoids in the Gredos massif, Spain: inferences from Sr-Nd isotopes.
909 Contributions to Mineralogy and Petrology 120, 137-149.

Murphy, J.B., Gutiérrez-Alonso, G., Fernández-Suárez, J., Braid, J.A., 2008. Probing crustal and mantle lithosphere origin through Ordovician volcanic rocks along the Iberian passive margin of Gondwana. Tectonophysics, 461, 166-180.

Nance, R.D., Gutiérrez-Alonso, G., Keppie, J.D., Linnemann, U., Murphy, J.B., Quesada, C., Strachan, R.A., Woodcock, N.H., 2010. Evolution of the Rheic Ocean. Gondwana Research 17, 194–222.

Navidad, M., 1978. Significado petrológico y geoquímico de las series glandulares en los sectores Nord-occidental y central del Macizo Ibérico. Ph.D. thesis, University Complutense de Madrid.

Navidad, M., Castiñeiras, P., Casas, J.M., Liesa, M., Fernández-Suárez, J., Barnolas, A., Carreras, J., Gil-Peña, I., 2010. Geochemical characterization and isotopic age of Caradocian magmatism in the northeastern Iberian Peninsula: Insights into the Late Ordovician evolution of the northern Gondwana margin. Gondwana Research 17, 325–337.

Neiva, A.M.R., Williams, I.S., Ramos, J.M.F., Gomes, M.E.P., Silva, M.M.V.G., Antunes, I.M.H.R., 2009. Geochemical and isotopic constraints on the petrogenesis of Early Ordovician granodiorite and Variscan two-mica granites from the Gouveia area, central Portugal. Lithos 111, 186–202.

Parga Pondal, I., Matte, P., Capdevila, R., 1964. Introduction à la géologie de l'Ollo de Sapo, formation porphyroide anté-silurienne du Nord-Ouest de l'Espagne. Notas y Comunicaciones del Instituto Geológico y Minero de España 76, 119–153.

Paterson, S.R., Okaya, D., Memeti, V., Economos, R., Miller, R.B., 2011. Magma addition and flux calculations of incrementally constructed magma chambers in continental margin arcs: combined field, geochronologic, and thermal modeling studies. Geosphere 7, 1439–1468.

Pereira, M.D., 1993. Termobarometría de rocas con la asociación granate–cordierita-biotita; trayectorias P–T en el complejo anatéctico de la Peña Negra (Batolito de Ávila).

943 Implicaciones sobre el metamorfismo hercínico en la Zona Centro Ibérica. Revista de la
944 Sociedad Geológica de España 6, 131–140.
945
946 Pereira, M.D., Bea, F., 1994. Cordierite-producing reactions in the Peña Negra complex, Avila
947 batholith, Central Spain: the key role of cordierite in low-pressure anatexis. Canadian
948 Mineralogist 32, 763–780.
949
950 Pereira, M.F., Linnemann, U., Hofmann, M., Chichorro, M., Solá, A.R., Medina, J., Silva, J.B.
951 2012. The provenance of Late Ediacaran and Early Ordovician siliciclastic rocks in the
952 Southwest Central Iberian Zone: constraints from detrital zircon data on northern Gondwana
953 margin evolution during the late Neoproterozoic. Precambrian Research 192–195; 166– 189.
954
955 Pereira, M.F., 2014. Potential sources of Ediacaran strata of Iberia: a review. Geodinamica Acta, 27
956 (1), 1-14. DOI: 10.1080/09853111.2014.957505.
957
958 Pin, C., Ortega Cuesta, L.A., Gil Ibarguchi, J.I., 1992. Mantle-derived, early Paleozoic A-type
959 metagranitoids from the NW Iberian Massif: Nd isotope and trace-element constraints.
960 Bulletin de la Societé Géologique de France 163, 483–494.
961
962 Rodríguez Alonso, M.D., Díez Balda, M.A., Perejón, A., Pieren, A., Liñán, E., López Díaz, F.,
963 Moreno, F., Gámez Vintaned, J.A., González Lodeiro, F., Martínez Poyatos, D., Vegas, R.,
964 2004. Dominio del Complejo Esquisto-grauváquico. Estratigrafía. La secuencia
965 litoestratigráfica del Neoproterozoico-Cámbrico inferior. In: Vera, J.A. (Ed.), Geología de
966 España. IGME-SGE, Madrid, pp. 78–81.
967
968 Romão, J., Dunning, G., Marcos, A., Dias, R., Ribeiro, A., 2010. The Mação-Penhascoso laccolith
969 granite: age and implications (SW-Central Iberian Zone). e-Terra 16, 1-4.
970
971 Rubio-Ordóñez, A., Valverde-Vaquero, P., Corretgé, L.G., Cuesta-Fernández, A., Gallastegui, G.,
972 Fernández-González, M., Gerdes, A., 2012. An Early Ordovician tonalitic–granodioritic belt
973 along the Schistose-Greywacke Domain of the Central Iberian Zone (Iberian Massif,
974 Variscan Belt). Geological Magazine 149 (5), 927–939.
975

976 Sánchez Martínez, S., Gerdes, A., Arenas, R., Abati, J., 2012. The Bazar ophiolite of NW Iberia: a
977 relic of the Iapetus-Tornquist Ocean in the Variscan suture. Terra Nova 24, 283-294.
978
979 Sánchez-García, T., Bellido, F., Pereira, M.F., Chichorro, M., Quesada, C., Pin, C., Silva, J.B.,
980 2010. Rift-related volcanism predating the birth of the Rheic Ocean (Ossa-Morena zone, SW
981 Iberia). Gondwana Research 17, 392–407.
982
983 Solá, A.R., Montero, P., Ribeiro, M.L., Neiva, A.M.R., Zinger, T., Bea, F., 2005. Pb/Pb age of the
984 Carrascal Massif, central Portugal. Geochimica et Cosmochimica Acta 69 (10, Supplement
985 1, Goldschmidt Conference Abstracts).
986
987 Solá, A.R., 2007. Relações Petrogeoquímicas dos Maciços Graníticos do NE Alentejano.
988 Unpublished Ph.D. dissertation, Universidade de Coimbra, Portugal, 405 pp.
989
990 Solá, A.R., Pereira, M.F., Williams, I.S., Ribeiro, M.L., Neiva, A.M.R., Montero, P., Bea, F.,
991 Zinger, T., 2008. New insights from U-Pb zircon dating of Early Ordovician magmatism on
992 the northern Gondwana margin: The Urra Formation (SW Iberian Massif, Portugal).
993 Tectonophysics 461, 114–29.
994
995 Stampfli, G.M., Borel, G.D., 2002. A plate tectonic model for the Paleozoic and Mesozoic
996 constrained by dynamic plate boundaries and restored synthetic oceanic isochrons. Earth
997 and Planetary Science Letters 196, 17–33.
998
999 Talavera, C., 2009. Pre-Variscan magmatism of the Central Iberian Zone: chemical and isotope
1000 composition, geochronology and geodynamic significance. Ph.D. Thesis, University of
1001 Granada, 252 pp.
1002
1003 Talavera, C., Montero, P., Bea, F., González-Lodeiro, F., Whitehouse, M., 2013. U-Pb zircon
1004 geochronology of the Cambro-Ordovician metagranites and metavolcanic rocks of central
1005 and NW Iberia. International Journal of Earth Sciences 102, 1-23.
1006
1007 Ugidos, J.M., Armenteros, I., Barba, P., Valladares, M.I., Colmenero, J.R., 1997a. Geochemistry
1008 and petrology of recycled orogen-derived sediments: a case study from Upper Precambrian

siliciclastic rocks of the Central Iberian Zone, Iberian Massif, Spain. Precambrian Research 84 (3–4), 163–180.

Ugidos, J.M., Valladares, M.I., Recio, C., Rogers, G., Fallick, A.E., Stephens, W.E., 1997b. Provenance of Upper Precambrian–Lower Cambrian shales in the Central Iberian Zone, Spain: evidence from a chemical and isotopic study. Chemical Geology 136, 55–70.

Ugidos, J.M., Valladares, M.I., Barba, P., 2001. Geochemistry of Precambrian–Cambrian Sedimentary Series in the Central Iberian Zone and Geological Implications: State of the Art. Abstracts Congreso Ibérico de Geoquímica, Zaragoza, Instituto Tecnológico de Aragón, pp. 175–184.

Valladares, M.I., Barba, P., Ugidos, J.M., Colmenero, J.R., Armenteros, I., 2000. Upper Neoproterozoic–Lower Cambrian sedimentary successions in the Central Iberian Zone (Spain): sequence stratigraphy, petrology and chemostratigraphy. Implications for other European zones. International Journal of Earth Sciences 89, 2–20.

Valverde-Vaquero, P., Dunning, G.R., 2000. New U–Pb ages for Early Ordovician magmatism in central Spain. Journal of the Geological Society of London 157, 15–26.

Valverde-Vaquero, P., Marcos, A., Farias, P., Gallastegui, G., 2005. U–Pb dating of Ordovician felsic volcanism in the schistose domain of the Galicia-Trás-os-Montes zone near Cabo Ortegal (NW Spain). Geol. Acta 3, 27–37.

Villaseca, C., Downes, H., Pin, C., Barbero, L., 1999. Nature and composition of the lower continental crust in central Spain and the granulite–granite linkage: inferences from Granulitic xenoliths. Journal of Petrology 40, 1463–1496.

Villaseca, C., Merino, E., Oyarzun, R., Orejana, D., Pérez-Soba, C., Chicharro, E., 2014. Contrasting chemical and isotopic signatures from Neoproterozoic metasedimentary rocks in the Central Iberian Zone (Spain) of pre-Variscan Europe: Implications for terrane analysis and Early Ordovician magmatic belts. Precambrian Research 245, 131-145.

Villaseca, C., Castiñeiras, P., Orejana, D., 2015. Early Ordovician metabasites from the Spanish

Central System: a remnant of intraplate HP rocks in the Central Iberian Zone. Gondwana Res. 27, 392–409.

van Staal, C.R., Dewey, J.F., MacNiocaill, C., McKerrow, W.S., 1998. The Cambrian–Silurian tectonic evolution of the northern Appalachians and British Caledonides: history of a complex, best and southwest Pacific-type segment of Iapetus. In: Blundell, D.J., Scott, A.C. (Eds.), Lyell: The Past is the Key to the Present. Geological Society of London Special Publications 143, 199–242.

Vogt, K., Gerya, T.V., Castro, A., 2012. Crustal growth at active continental margins: numerical modeling. Physics of the Earth and Planetary Interiors 192-193, 1-20.

Wang, X., Griffin, W.L., Chen, J., Huang, P., Li, X., 2011. U and Th contents and Th/U ratios of zircon in felsic and mafic magmatic rocks: improved zircon-melt distribution coefficients. Acta Geologica Sinica 85, 164–174.

Williams, I.S., Claesson, S., 1987. Isotopic evidence for the Precambrian provenance and Caledonian metamorphism of high grade paragneisses from the Seve Nappes, Scandinavian Caledonides, II Ion microprobe zircon U–Th–Pb. Contributions to Mineralogy and Petrology 97, 205–217.

Williams, I.S., 1998. U–Th–Pb geochronology by ion microprobe. In: McKibben, M.A., Shanks III, W.C., Ridley, W.I. (Eds.), Applications of Microanalytical Techniques to Understanding Mineralizing Processes: Reviews in Economic Geology, 7, pp. 1–35.

Winchester, J.A., Pharaoh, T.C., Verniers, J., 2002. Palaeozoic amalgamation of Central Europe: an introduction and synthesis of new results from recent geological and geophysical investigations. In: Palaeozoic Amalgamation of Central Europe. In: Winchester, J.A., Pharaoh, T.C., Verniers, J. (Eds.), Geological Society of London Special Publications, 201, pp. 1–18.

Yenes, M., Álvarez, F., Gutiérrez-Alonso, G., 1999. Granite emplacement in orogenic compressional conditions: the La Alberca–Béjar granitic area (Spanish Central System, Variscan Iberian Belt). Journal of Structural Geology 21, 1419–1440.

Zeck, H. P., Wingate, M. T. D., Pooley, G. D., Ugidos, J. M., 2004. A Sequence of Pan-African and Hercynian Events Recorded in Zircons from an Orthogneiss from the Hercynian Belt of Western Central Iberia – an Ion Microprobe U–Pb Study. Journal of Petrology 45, 1613–1629.

Figure captions

Figure 1. (a) Geological sketch of the Iberian Massif indicating in black color the main occurrences of Cambro-Ordovician igneous rocks. The black box indicates the location of the studied area. Abbreviations: CZ: Cantabrian Zone, WALZ: Western Asturian-Leonese Zone, GTMZ: Galicia-Trás-os-Montes Zone, CIZ: Central Iberian Zone, OMZ: Ossa-Morena Zone, SPZ: South-Portuguese Zone. SGC: Schist and Greywacke Complex. (b) Geological map of the central area of the Spanish Central System batholith (see location in Fig. 1a) indicating the location of the Gredos massif and the studied area. (c) Detailed geological map of Prado de las Pozas in central Gredos (see location in Fig. 1b).

Figure 2. (a) Crd-Leucogranite layer in Prado de las Pozas. Its most outstanding feature is the presence of Crd nodules (some Bt can also be seen) oriented parallel to the main foliation in the leucogranite layer. (b) Medium- to fine-grained nebulites with a huge number of Bt-Crd-Sil restites. (c) Large-size Bt-Crd-Sil restite. (d) Large Kfs nodules (6-10 cm in diameter) in nodular granites and nebulites. (e) Roof contact between nodular granites (to the right) and the intrusive granitoids (to the left) in Prado de las Pozas (Las Pozas layer, Díaz-Alvarado et al., 2011). The contact, 4-6 m wide, consists of several interbedded sheets of Crd-monzogranites (including Kfs megacrysts and mafic microgranular enclaves) and nodular granites (including Crd and Kfs nodules, and leucogranite bands). (f) Qtz-diorite enclaves in nebulites. They show lobulate contacts and variably sized fragments. Qtz-diorite enclaves showing lenticular or ellipsoidal shapes also occur in Crd-leucogranite layers.

Figure 3. Geochemical features of Prado de las Pozas samples (central Gredos massif). For comparison, main units representing the Cambro-Ordovician magmatism and the Neoproterozoic metasedimentary rocks of the Iberian Massif are included. a) FeOt/FeOt+CaO vs SiO_2. b) ASI (Alumina Saturation Index) vs SiO_2. c) A–B diagram by Debon and Le Fort (1983, 1988). d) CaO

vs MgO diagram showing the trends drawn by calc-alkaline magmatic associations (LLD: Liquid Lines of Descent) (Castro, 2013b), and leucogranites. e) F–An–Or plot (Castro, 2013b) including the geochemical cotectic evolution of cordilleran granitoids and leucogranites. Greywackes and pelites fields are marked for comparison with Gredos massif samples. 1- Central Gredos samples (Díaz-Alvarado et al., 2011). 2- Average Ollo de Sapo (Iberia). Compilation from Fernández et al. (2008). 3- Hiendelaencina and Villadepera metavolcanic rocks and Antoñita and Miranda do Douro gneisses from Montero et al. (2007). 4- Urra Formation volcaniclastic rocks (Solá et al., 2008). 5- Outlined fields for Ollo de Sapo and Neoproterozoic sediments (SGC) in Iberia are obtained from García de Figuerola (1966), Capdevila (1969), Gil Ibarguchi (1978), Navidad (1978), Holtz (1987), Beetsma (1995), Briggs (1995), Ugidos et al. (1997a,b, 2001), Valladares et al. (2000), Castro et al. (2000, 2003), Corretgé et al. (2001), Bea et al. (2003).

Figure 4. Cathodoluminescence images of some of the zircons from the three samples selected for the SHRIMP U–Th–Pb analysis. Spots location and $^{206}Pb/^{238}U$ ages are indicated. Data are given in Table 3. Scale bars (white lines) are 100 μm.

Figure 5. (a) U–Pb Concordia diagrams of the nodular granite sample (J706-43). Error ellipses in Concordia diagrams represent a 68.3% conf., including the standard error. (b) Enlarged area for Neoproterozoic and Paleozoic ages and including analyses from all samples. (c) Chronological chart representing the age of most relevant Cambro-Ordovician geological units of the Iberian Massif in the upper part. These data are compared with the set of Cambro-Ordovician ages yielded by nodular granites and Qtz-dioritic enclaves in the lower part. 1: Montero et al. (2007); 2: Solá et al. (2008); 3: Solá (2007); 4: Solá et al. (2005); 5: Rubio-Ordóñez et al. (2012).

Figure 6. Probability density plots of U-Th-Pb zircon ages obtained from nodular granites (J706-43) and late Neoproterozoic to Ordovician reference domains of the Central Iberian Zone (CIZ). a) Probability distribution of $^{206}Pb/^{238}U$ ages of nodular granites. $^{207}Pb/^{206}Pb$ are preferred for ages older than 1 Ga. Main peaks are noted for further comparison. b) Probability plot of detrital zircon ages from late Neoproterozoic greywackes (Beiras Group) and Early Ordovician quartzites (Sarnelhas and Armorican Quarzite formations) of SW CIZ. Grey vertical lines indicate the major probability peaks in the nodular granite sample. c) U-Pb age distribution of metagranites and metavolcanic rocks from Ollo de Sapo Domain and Central Iberian and NW Iberian gneisses of North CIZ. Major peaks observed in the nodular granite sample are included. N: number of analysis. 1: This study; 2: Pereira et al. (2012); 3: Talavera et al. (2013) and references therein.

Figure 7. Schematic cross-section (not to scale) depicting a tectonic model for the origin of the Cambro-Ordovician magmatism of the Central Iberian Zone (Iberian Massif). Cold diapirs rooted in the subduction mélange (e.g. Gerya and Yuen, 2003, Castro and Gerya, 2008) ascended through the mantle wedge and accumulated at the basal part of the lithosphere, giving place to partially molten resevoirs of mafic or intermediate to felsic magmas (e.g. Castro and Gerya, 2008, Castro et al., 2010, Hacker et al., 2011) and feeding the magmatic arc and the extensional back-arc region. Cold diapirs made by molten sediments predominated at the back-arc region. The arc-back-arc setting shown in the section is inspired in similar interpretative sketches for this Cambro-Ordovician event published by Fernández et al. (2008), Rubio Ordóñez et al. (2012) and Villaseca et al. (2014).

Table 1

Click here to download Table: Table 1.docx

Table 1
Summary of geochronological data of the Cambro-Ordovician magmatism in the Iberian Massif.

Rock type	Geological location	Crystallization age (Ma)	Analytical method	Reference
Metavolcanic rocks (Ollo de Sapo)	Villadepera (Ollo de Sapo Domain, NW Iberia)	483 ±4	Zrn U-Pb ion microprobe and LA-ICPMS and Pb-Pb TIMS	Montero et al. (2007)
Metavolcanic rocks (Ollo de Sapo)	Hiendelaencina (Ollo de Sapo Domain, central Iberia)	495 ±5 - 483 ±3	Zrn U-Pb ion microprobe and LA-ICPMS and Pb-Pb TIMS	Montero et al. (2007)
Metavolcanic rocks and Metagranites (Ollo de Sapo)	Sanabria, Trives and Vivero (NW Ollo de Sapo Domain)	492 ±4 - 486 ±5	Zrn U-Th–Pb ion microprobe and LA-ICPMS	Montero et al. (2009)
Metagranite (miranda do Douro)	Villadepera (Ollo de Sapo Domain, NW Iberia)	483 ±3	Zrn U-Pb ion microprobe and LA-ICPMS	Bea et al. (2006)
Metagranite (Antoñita)	Hiendelaencina (Ollo de Sapo Domain, central Iberia)	474 ±4	Zrn U-Pb ion microprobe and LA-ICPMS and Pb-Pb TIMS	Montero et al. (2007)
San Sebastian metagranite (Ollo de Sapo)	Sanabria (NW Ollo de Sapo Domain)	470 ±3	Zrn U-Th–Pb ion microprobe and LA-ICPMS	Montero et al. (2009)
Ignimbrite	Sanabria (NW Ollo de Sapo Domain)	488 ±6	Zrn U-Pb TIMS	Díez-Montes et al. (2010)
Augen gneiss	Sanabria (NW Ollo de Sapo Domain)	472 ±14	Zrn U-Pb TIMS	Díez-Montes et al. (2010)
Metagranites ("Galician" gneisses)	Several locations (Galicia Trás-os-Montes Zone)	497 ±6 - 462 ±8	Zrn U-Th–Pb ion microprobe and LA-ICPMS	Talavera et al. (2013)
Granodiorite orthogneiss	Malpica-Tui Complex (Galicia Trás-os-Montes Zone)	489 ±4	Zrn U–Th–Pb SHRIMP-RG	Díez Fernández et al. (2012b)
Alkali-granite orthogneiss	Malpica-Tui Complex (Galicia Trás-os-Montes Zone)	474 ±3	Zrn U–Th–Pb SHRIMP-RG	Díez Fernández et al. (2012b)
Alkaline and peralkaline granite gneiss	Malpica-Tui Complex (Galicia Trás-os-Montes Zone)	475-470	Zrn U–Th–Pb SHRIMP-RG	Díez Fernández et al. (2012b)
Metavolcaniclastic rocks (rhyolites and dacites)	Bragança–Alcañices area (Galicia Trás-os-Montes Zone)	500 ±4 - 489 ±4	Zrn U–Th–Pb SHRIMP	Farias et al. (2014)
Alkaline metarhyolite	Queiroga Series (Galicia Trás-os-Montes Zone)	475 ±2	Zrn U-Pb LA-MC-ICPMS	Valverde-Vaquero et al. (2005)
Calc-alkaline rhyolites	Eastern Galicia-Trás-os-Montes Zone	455	Zrn U-Pb LA-MC-ICPMS	Dias da Silva et al. (2015)
K-bentonites (Super-eruption?)	Several locations (NW Iberia, Cantabrian Zone)	477 ±1	Zrn and Mnz U–Pb ID-TIMS	Gutiérrez-Alonso et al. (2016)
Metagranites ("Castilian" gneisses)	Several locations (Central Iberian Zone)	498 ±4 - 471 ±7	Zrn U-Th–Pb ion microprobe and LA-ICPMS	Talavera et al. (2013)
Intraplate basalt	Central Iberian Zone	455	Zrn U-Pb LA-MC-ICPMS	Dias da Silva et al. (2015)
Meta-tholeiites	Tenzuela (Central Iberian Zone)	473 ±2	Zrn U–Th–Pb SHRIMP	Villaseca et al. (2015)
Anatectic rocks	Sotosalvos (Central Iberian Zone)	480 - 464 ±3 (Pre-Hercynian ages)	Zrn U–Th–Pb SHRIMP-RG	Castiñeiras et al. (2008)
Tonalites and granodiorites (Beira Baixa–Central Extremadura tonalite belt)	Zarza la Mayor (SW Central Iberian Zone)	478 ±1	Zrn U–Pb LA-ICPMS and ID-TIMS	Rubio-Ordóñez et al. (2012)
Tonalites and granodiorites (Beira Baixa–Central Extremadura tonalite belt)	Arroyo de la Luz and Zarza de Montánchez (SW Central Iberian Zone)	470 ±15 and 482 ±10	Mnz EMPA	Rubio-Ordóñez et al. (2012)
Tonalite/granodiorite and Bt+Ms granites (Beira Baixa–Central Extremadura tonalite belt)	Oledo (SW Central Iberian Zone)	481 ±1 - 478 ±1	Zrn and Mnz U–Pb ID-TIMS	Antunes et al. (2009)
Porphyritic felsic volcanoclastic rocks (Urra Formation)	Urra (Central Iberian/Ossa-Morena transition zone)	495 ±7 - 488 ±5	Zrn U–Th–Pb SHRIMP	Solá et al. (2008)
Gabbros, diorites and granites (Beira Baixa–Central Extremadura tonalite belt)	Carrascal (Central Iberian/Ossa-Morena transition zone)	486 - 471	Zrn Pb-Pb TIMS	Solá et al. (2005)
Granites (Beira Baixa–Central Extremadura tonalite belt)	Portalegre (Central Iberian/Ossa-Morena transition zone)	493 ±4	Zrn U-Pb SHRIMP	Solá (2007)

Table 2

Click here to download Table: Table 2.docx

Table 2: Whole rock compositions of the main facies in the high-grade metamorphic complex in Prado de las Pozas (Gredos Massif) and comparative Cambro-Ordovician igneous rocks in Iberia

Location	Prado de las Pozas (Gredos Massif)					Gredos massif			Iberia		Hiendelaencina and Villadepera				Antoñita and Miranda do Douro					Urra Formation						
Reference	Díaz-Alvarado et al. (2011)			This study		Díaz-Alvarado et al. (2011)			Fernández et al. (2008)		Montero et al. (2007)				Montero et al. (2007)					Sola et al. (2008)						
Rock type	Nodular granite	Qtz-Diorite	Nebulite	Crd-leucogranite	Metasediment enclave	Hornfels			Ollo de Sapo Average (N=95)	SGC Average (N=68)	Metavolcanic rock				Gneiss					Porphyritic volcaniclastic rock						
Sample	J-706-43	J809-13	J809-10	J809-15	J809-11	J-707-8	J-707-7	J709-2			CT6	CT7	GNB9	GNB8	CT4	CT10	CT11	CT9	GNB11	URRA 2	URRA 5	URRA 8	URRA 4	URRA 7	URRA 1	URRA 3
wt %																										
SiO2	68,31	61,05	63,74	72,19	58,98	56,69	61,86	57,84	67,53	64,16	68,06	71,92	68,02	70,67	76	71,46	72,37	70,25	64,62	66,7	69,02	70,14	70,79	71,53	74,53	75,43
TiO2	0,50	1,15	0,72	0,35	1,07	0,81	0,65	0,91	0,55	0,84	0,5	0,4	0,68	0,54	0,09	0,32	0,35	0,43	0,62	0,83	0,43	0,44	0,46	0,47	0,18	0,16
Al2O3	15,51	17,64	17,23	14,68	18,92	21,03	19,21	20,45	15,79	17,64	15,76	14,81	15,34	14,44	12,88	14,45	13,92	15,07	16,07	15,91	16,12	15,63	15,27	14,99	13,6	13,12
FeOt	3,85	5,75	5,41	1,96	7,87	6,88	4,71	7,65	3,77	6,08	3,32	2,59	3,73	3,45	1,14	2,1	2,36	2,61	3,83	4,92	2,81	2,71	2,43	2,75	1,84	1,63
MgO	1,37	2,21	2,03	0,64	3,36	2,95	1,83	3,44	1,56	2,12	1,49	1,18	1,44	0,92	0,12	0,59	0,77	0,89	2,23	1,81	1,05	1	0,85	0,9	0,39	0,49
MnO	0,06	0,08	0,07	0,02	0,10	0,08	0,06	0,16	0,04	0,04	0,04	0,02	0,05	0,04	0,01	0,03	0,03	0,04	0,06	0,04	0,02	0,02	0,01	0,03	0,02	0,03
CaO	0,87	4,44	0,69	0,47	1,08	0,35	0,58	0,60	1,19	0,27	1,38	1,03	1,28	1,08	0,41	0,8	1,08	0,91	2,93	0,75	0,39	0,31	0,41	0,33	0,46	0,24
Na2O	2,58	3,24	2,23	3,41	2,47	1,65	3,13	1,64	2,86	1,55	2,73	2,85	2,17	3,35	2,29	2,74	3,14	2,55	3,21	3,08	3,28	2,5	2,54	2,53	2,41	2,21
K2O	4,19	2,29	4,30	4,45	3,32	4,21	3,44	4,25	4,18	3,43	4,18	3,14	4,39	4,08	5,83	5,27	4,28	5,39	4,03	2,58	4,37	4,6	4,09	4,02	4,77	5,17
P2O5	0,12	0,25	0,29	0,24	0,15	0,16	0,24	0,17	0,17	0,15	0,18	0,16	0,25	0,19	0,15	0,17	0,17	0,2	0,35	0,2	0,21	0,21	0,21	0,19	0,22	0,12
Loi	1,48	0,81	2,32	1,18	1,74	3,92	3,26	1,76	1,9	1,63	1,43	1,18	1,82	0,82	0,53	1,11	0,85	0,97	1,6	2,47	1,95	1,94	2,43	1,83	1,32	1,1
Total	98,84	99,62	99,68	99,82	100,1	98,73	98,97	99,81	99,80	98,03	99,07	99,28	99,17	99,58	99,45	99,04	99,32	99,31	99,55	99,84	99,97	99,81	99,76	99.88	99,95	99,88
Zr (ppm)	134,1	210,4	238,7	97,20	222,3																					

Table 3

Click here to download Table: Table 3.doc

Table 3

Summary of SHRIMP U-Pb zircon data for the selected samples

		ppm					Isotope ratios							Ages				
Id	Spot[(1)(2)]	U	Th	$^{206}Pb^*$	% $^{206}Pb_c$	Th/U	$^{207}Pb^*/^{206}Pb^*$	±%	$^{206}Pb^*/^{238}U$	±%	$^{207}Pb^*/^{235}U$	±%	err corr	$^{206}Pb/^{238}U$	±	$^{207}Pb/^{206}Pb$	±	% Disc.
J706-43: Nodular granites																		
15.1	hlc,t2	62	28	24.9	0.01	0.458	0.1824	0.9	0.4643	2.1	11.68	2.2	0.923	2459	42	2675	14	8
15.2	r,t2	452	125	140	--	0.286	0.1529	0.4	0.3596	1.0	7.580	1.1	0.925	1980	18	2378	7.3	17
17.1	c,t2	1347	29	412	--	0.023	0.1222	0.2	0.3561	1.0	6.000	1.0	0.988	1964	17	1988	2.9	1
17.2	hlr,t2	60	40	18.4	--	0.681	0.1235	0.8	0.3556	1.3	6.053	1.5	0.854	1961	22	2007	14	2
17.3	r,t2	424	19	127	--	0.047	0.1215	0.5	0.3487	1.0	5.843	1.2	0.909	1928	17	1978	8.6	3
1.1	c,t2	170	179	20.8	--	1.080	0.0676	1.3	0.1419	1.2	1.323	1.8	0.681	856	9.9	856	27	0
2.1	hlc,t2	95	56	8.1	0.31	0.616	0.0602	2.1	0.0988	1.3	0.820	2.4	0.516	608	7.3	609	45	0
3.1	c,t2	115	77	10.0	--	0.694	0.0611	1.4	0.1011	1.2	0.851	1.9	0.655	621	7.2	642	30	3
6.1	r,t2	3350	1056	299	0.02	0.326	0.0611	0.3	0.1040	1.0	0.876	1.1	0.971	638	6.3	644	5.5	1
9.1	hlc,t2	30	72	2.6	0.22	2.530	0.0610	3.0	0.1013	1.7	0.852	3.4	0.495	622	10	640	64	3
10.1	r,t2	531	170	46.5	0.01	0.331	0.0610	0.7	0.1020	1.1	0.858	1.2	0.847	626	6.3	640	14	2
11.1	r,t2	1069	175	99.7	0.19	0.169	0.0597	0.8	0.1084	1.0	0.891	1.3	0.795	663	6.5	591	17	-12
14.1	r,t2	746	434	67.1	--	0.601	0.0611	1.6	0.1048	1.1	0.883	1.9	0.546	642	6.5	643	35	0
16.1	c,t2	461	207	40.2	0.04	0.465	0.0606	0.7	0.1016	1.1	0.848	1.3	0.826	624	6.3	623	16	0
16.2	hlr,t2	77	59	6.6	--	0.800	0.0610	1.9	0.0995	1.8	0.837	2.6	0.697	611	11	640	40	5
7.1	c,t2	337	104	26.4	--	0.320	0.0588	0.9	0.0912	1.1	0.740	1.4	0.774	563	5.8	560	19	0
13.1	c,t2	626	543	50.7	--	0.897	0.0598	0.6	0.0943	1.1	0.778	1.2	0.855	581	5.9	597	14	3
19.1	t1a	360	182	28.6	0.08	0.521	0.0587	0.9	0.0924	1.5	0.747	1.7	0.868	570	8.1	555	19	-3
20.1	t1a	496	236	39.4	0.09	0.492	0.0589	0.7	0.0924	1.2	0.750	1.4	0.858	570	6.8	563	16	-1
23.1	t1b	921	566	73.2	0.16	0.635	0.0590	0.7	0.0923	1.2	0.751	1.4	0.882	569	6.7	567	14	0
1.2	r,t2	857	40	57.7	--	0.048	0.0578	0.7	0.0784	1.0	0.625	1.2	0.840	487	4.9	523	15	7
4.1	r,t2	523	37	35	--	0.072	0.0585	1.0	0.0780	1.1	0.629	1.5	0.716	484	5	548	23	12
5.1	r,t2	345	33	23	0.03	0.099	0.0566	1.0	0.0776	1.1	0.606	1.5	0.736	482	5.1	475	22	-1
21.1	t1a	334	179	21.1	0.12	0.553	0.0562	1.6	0.0735	1.3	0.570	2.0	0.624	457	5.6	460	35	1
11.2	r,t2	526	26	28.8	0.46	0.052	0.0548	2.0	0.0635	1.1	0.480	2.2	0.481	397	4.1	402	44	1
18.1	r,t2	595	24	28.6	0.07	0.042	0.0539	1.0	0.0559	1.2	0.415	1.6	0.774	350	4.3	368	23	5
3.2	r,t2	1677	15	78.8	0.58	0.009	0.0534	1.2	0.0544	1.0	0.400	1.6	0.641	341	3.4	344	28	1
8.1	t1a	226	175	10	--	0.799	0.0534	1.5	0.0515	1.2	0.378	1.9	0.606	323	3.7	344	34	6
9.2	r,t2	640	78	27.6	0.03	0.126	0.0532	0.9	0.0502	1.1	0.368	1.4	0.749	316	3.3	339	21	7
22.1	r,t2	863	5	36.8	0.02	0.006	0.0525	0.7	0.0496	1.3	0.359	1.4	0.874	312	3.9	306	16	-2
25.1	r,t2	792	3	33.4	0.07	0.004	0.0521	0.8	0.0490	1.2	0.352	1.5	0.833	308	3.7	290	19	-6
24.1	r,t2	1747	3	72.9	0.23	0.002	0.0526	0.7	0.0485	1.2	0.351	1.4	0.877	305	3.7	311	15	2
J809-13: Qtz-Diorite enclaves																		
1.1	t1a	420	43	28.3	0.52	0.105	0.0550	2.3	0.0779	2.4	0.591	3.3	0.718	483	11	412	51	-17
2.1	t1b	1375	68	90.1	0.07	0.051	0.0568	0.9	0.0762	2.3	0.597	2.5	0.935	473	11	485	19	2
3.1	t1b	1122	71	75.1	0.13	0.065	0.0556	1.0	0.0778	2.3	0.597	2.5	0.924	483	11	437	21	-11
4.1	c,t2	1214	174	125	0.06	0.148	0.0623	0.5	0.1195	2.3	1.027	2.4	0.978	728	16	685	11	-6
5.1	t1a	338	58	22.4	0.13	0.178	0.0576	1.4	0.0772	2.4	0.613	2.8	0.856	479	11	514	32	7
J809-15: Crd-Leucogranites																		
1.1	c,t2	640	378	67	0.29	0.61	0.0637	0.9	0.1215	2.5	1.066	2.7	0.929	739	17	730	21	-1
2.1	-	824	1241	31.5	0.27	1.556	0.0525	2.4	0.0444	2.5	0.321	3.4	0.723	280	6.8	308	54	9
3.1	c,t2	1545	314	110	0.43	0.21	0.0588	1.6	0.0827	2.3	0.671	2.8	0.828	512	11	560	34	8
4.1	r,t2	303	147	11.9	0.62	0.502	0.0527	3.3	0.0455	2.6	0.331	4.2	0.625	287	7.4	316	75	9

Errors are 1-sigma; Pbc and Pb* indicate the common and radiogenic portions, respectively. Error in standard calibration was 0.21% (J706-43), 1.18% (J809-13 and J809-15) (not included in the above errors but required when comparing data from different mounts).

Common Pb corrected using measured ^{204}Pb.

(1) c: core; r: rim; hl: high luminosity area.

(2) Zircon types. t1a: Simple acicular parallel banded zircon with high elongation ratio. t1b: Simple euhedral zircon with oscillatory concentric zoning. t2: Zircon composed by an inherited core and external overgrowths.

Figure 1

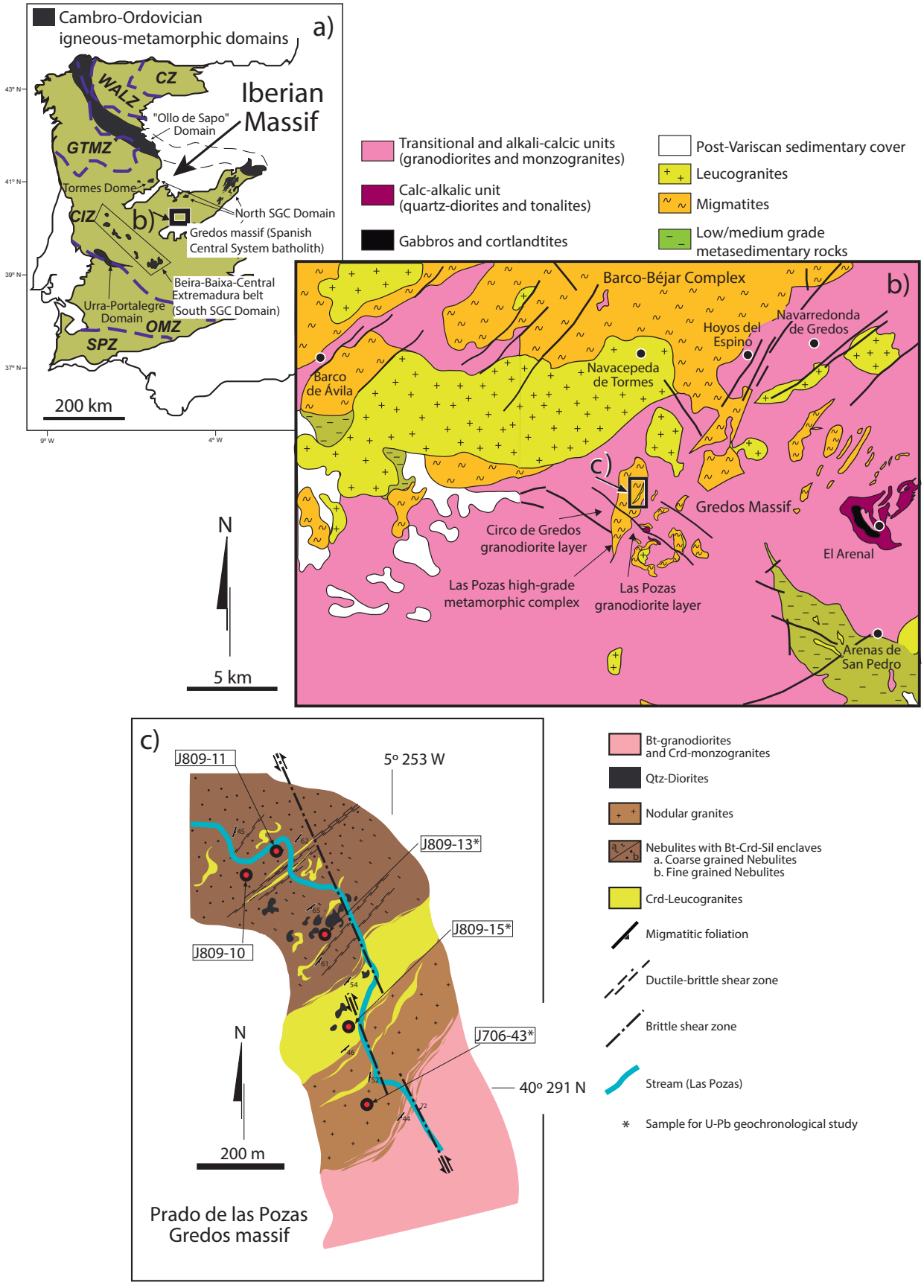

Figure 1. (a) Geological sketch of the Iberian Massif indicating in black color the main occurrences of Cambro-Ordovician igneous rocks. The black box indicates the location of the studied area. Abbreviations: CZ: Cantabrian Zone, WALZ: Western Asturian-Leonese Zone, GTMZ: Galicia-Trás-os-Montes Zone, CIZ: Central Iberian Zone, OMZ: Ossa-Morena Zone, SPZ: South-Portuguese Zone. SGC: Schist and Greywacke Complex. (b) Geological map of the central area of the Spanish Central System batholith (see location in Fig. 1a) indicating the location of the Gredos massif and the studied area. (c) Detailed geological map of Prado de las Pozas in central Gredos (see location in Fig. 1b).

Figure 2

Click here to download high resolution image

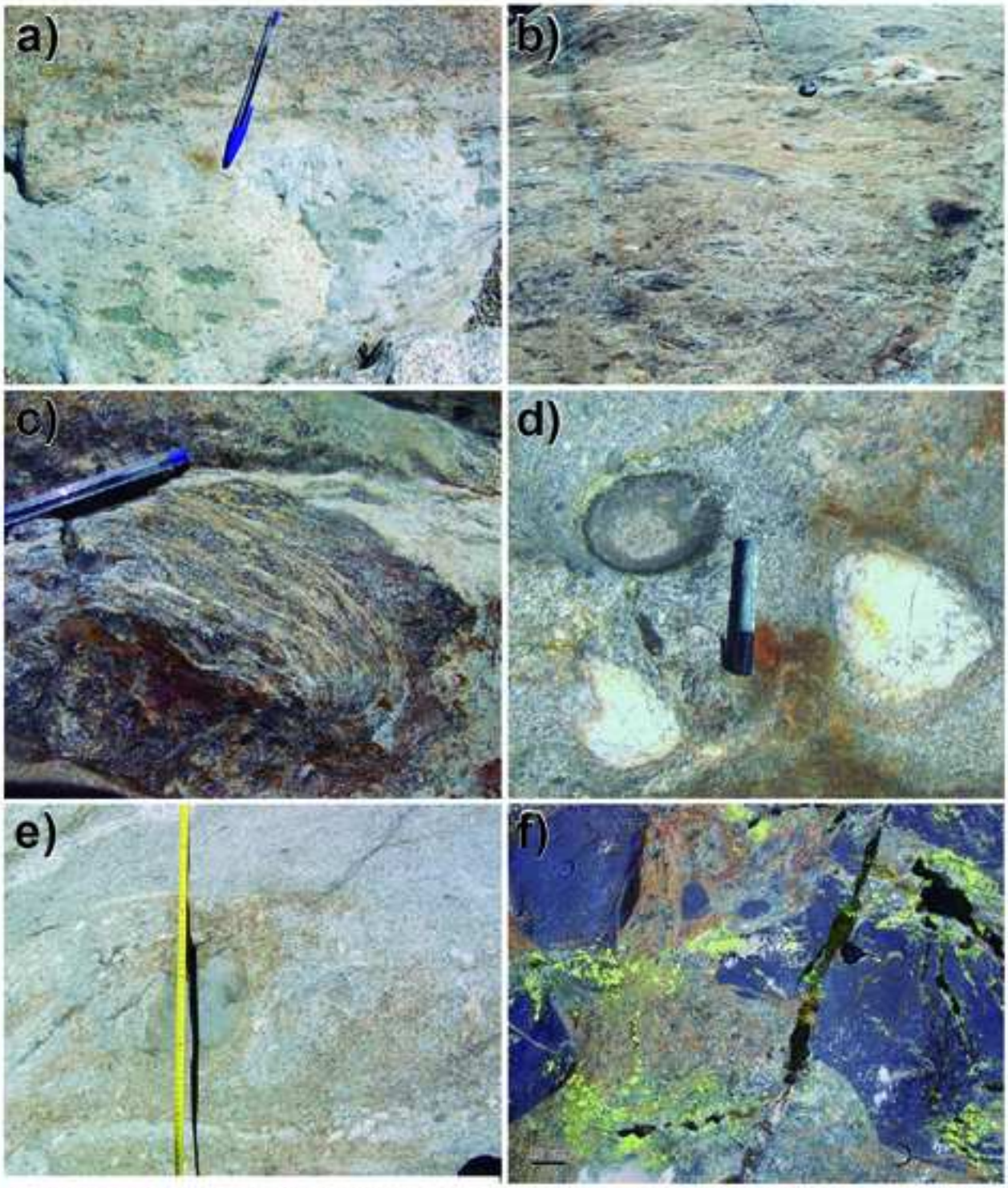

Figure 2. (a) Crd-Leucogranite layer in Prado de las Pozas. Its most outstanding feature is the presence of Crd nodules (some Bt can also be seen) oriented parallel to the main foliation in the leucogranite layer. (b) Medium- to fine-grained nebulites with a huge number of Bt-Crd-Sil restites. (c) Large-size Bt-Crd-Sil restite. (d) Large Kfs nodules (6-10 cm in diameter) in nodular granites and nebulites. (e) Roof contact between nodular granites (to the right) and the intrusive granitoids (to the left) in Prado de las Pozas (Las Pozas layer, Díaz-Alvarado et al., 2011). The contact, 4-6 m wide, consists of several interbedded sheets of Crd-monzogranites (including Kfs megacrysts and mafic microgranular enclaves) and nodular granites (including Crd and Kfs nodules, and leucogranite bands). (f) Qtz-diorite enclaves in nebulites. They show lobulate contacts and variably sized fragments. Qtz-diorite enclaves showing lenticular or ellipsoidal shapes also occur in Crd-leucogranite layers.

Figure 3

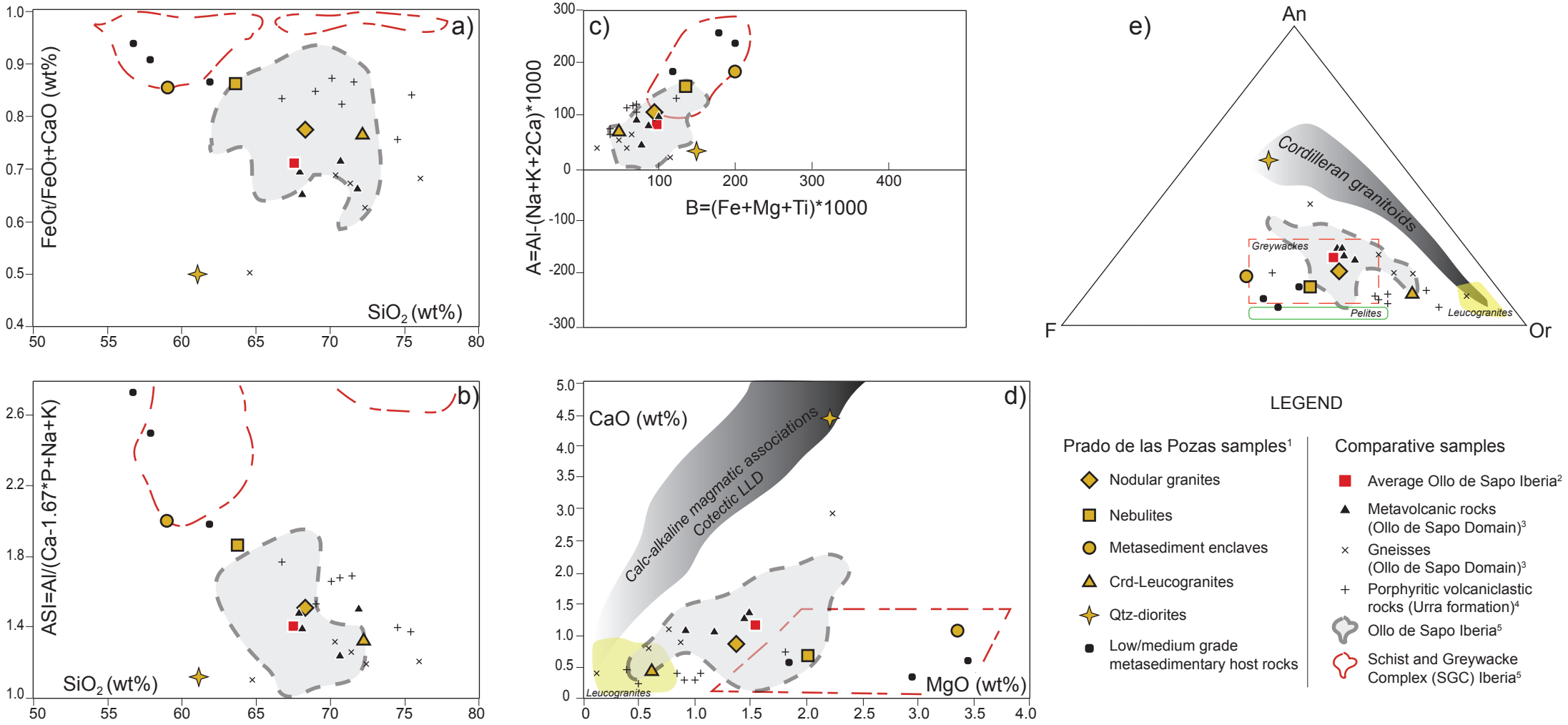

Figure 3. Geochemical features of Prado de las Pozas samples (central Gredos massif). For comparison, main units representing the Cambro-Ordovician magmatism and the Neoproterozoic metasedimentary rocks of the Iberian Massif are included. a) FeOt/FeOt+CaO vs SiO2. b) ASI (Alumina Saturation Index) vs SiO2. c) A–B diagram by Debon and Le Fort (1983, 1988). d) CaO vs MgO diagram showing the trends drawn by calc-alkaline magmatic associations (LLD: Liquid Lines of Descent) (Castro, 2013b), and leucogranites. e) F–An–Or plot (Castro, 2013b) including the geochemical cotectic evolution of cordilleran granitoids and leucogranites. Greywackes and pelites fields are marked for comparison with Gredos massif samples. 1- Central Gredos samples (Díaz-Alvarado et al., 2011). 2- Average Ollo de Sapo (Iberia). Compilation from Fernández et al. (2008). 3- Hiendelaencina and Villadepera metavolcanic rocks and Antoñita and Miranda do Douro gneisses from Montero et al. (2007). 4- Urra Formation volcaniclastic rocks (Solá et al., 2008). 5- Outlined fields for Ollo de Sapo and Neoproterozoic sediments (SGC) in Iberia are obtained from García de Figuerola (1966), Capdevila (1969), Gil Ibarguchi (1978), Navidad (1978), Holtz (1987), Beetsma (1995), Briggs (1995), Ugidos et al. (1997a,b, 2001), Valladares et al. (2000), Castro et al. (2000, 2003), Corretgé et al. (2001), Bea et al. (2003).

Figure 4

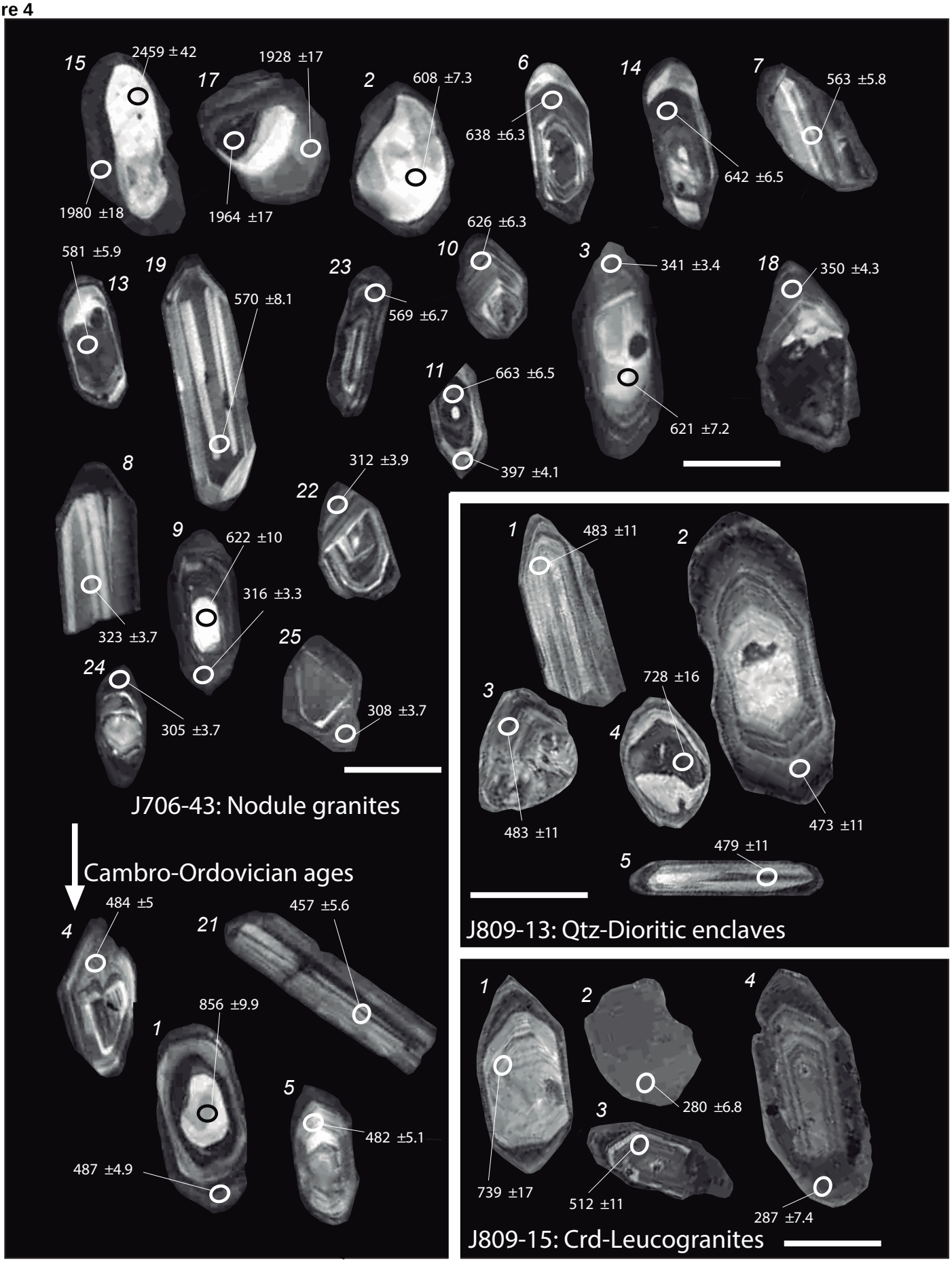

Figure 4. Cathodoluminescence images of some of the zircons from the three samples selected for the SHRIMP U–Th–Pb analysis. Spots location and 206Pb/238U ages are indicated. Data are given in Table 3. Scale bars (white lines) are 100 μm.

Figure 5

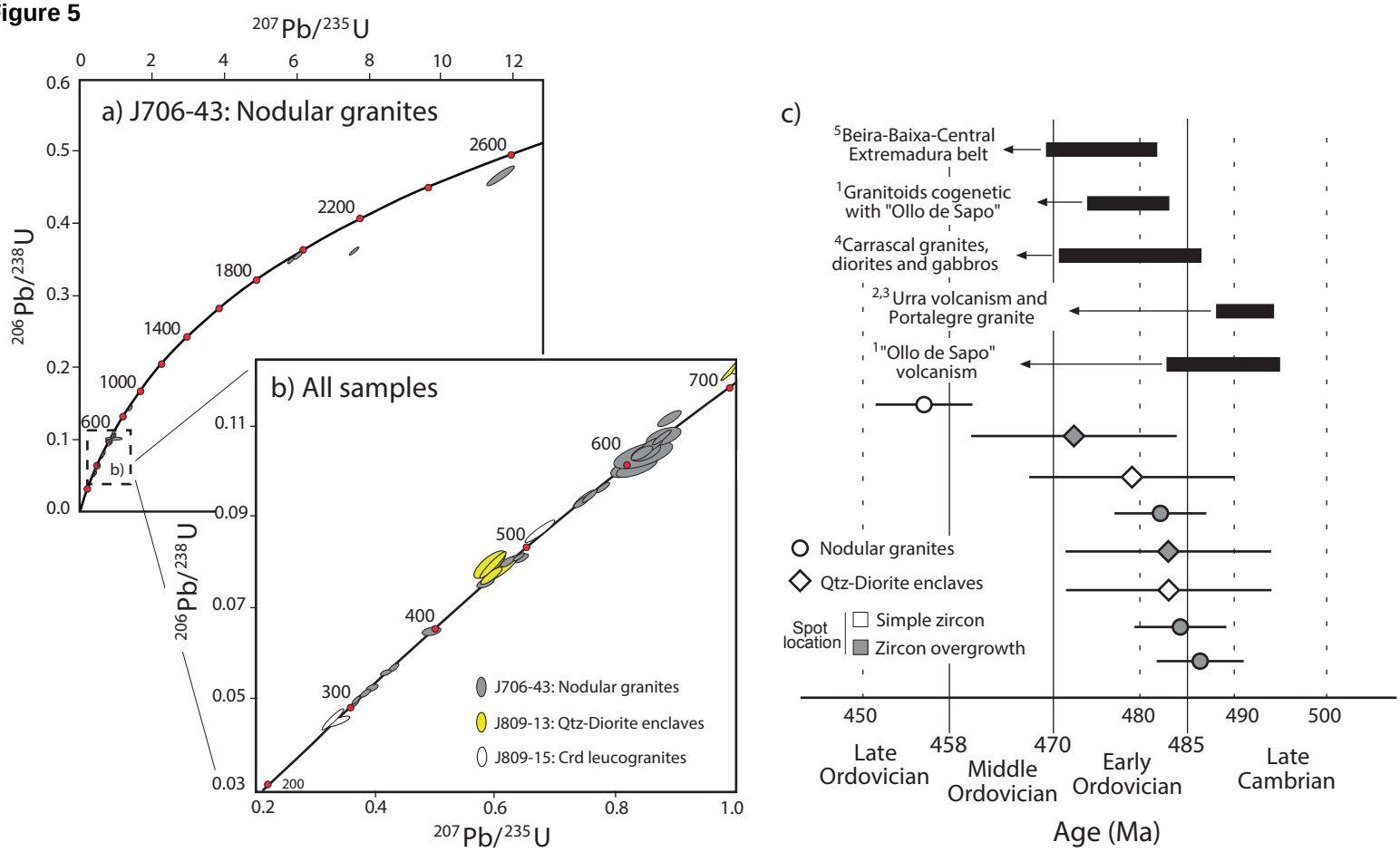

Figure 5. (a) U–Pb Concordia diagrams of the nodular granite sample (J706-43). Error ellipses in Concordia diagrams represent a 68.3% conf., including the standard error. (b) Enlarged area for Neoproterozoic and Paleozoic ages and including analyses from all samples. (c) Chronological chart representing the age of most relevant Cambro-Ordovician geological units of the Iberian Massif in the upper part. These data are compared with the set of Cambro-Ordovician ages yielded by nodular granites and Qtz-dioritic enclaves in the lower part. 1: Montero et al. (2007); 2: Solá et al. (2008); 3: Solá (2007); 4: Solá et al. (2005); 5: Rubio-Ordóñez et al. (2012).

Figure 6

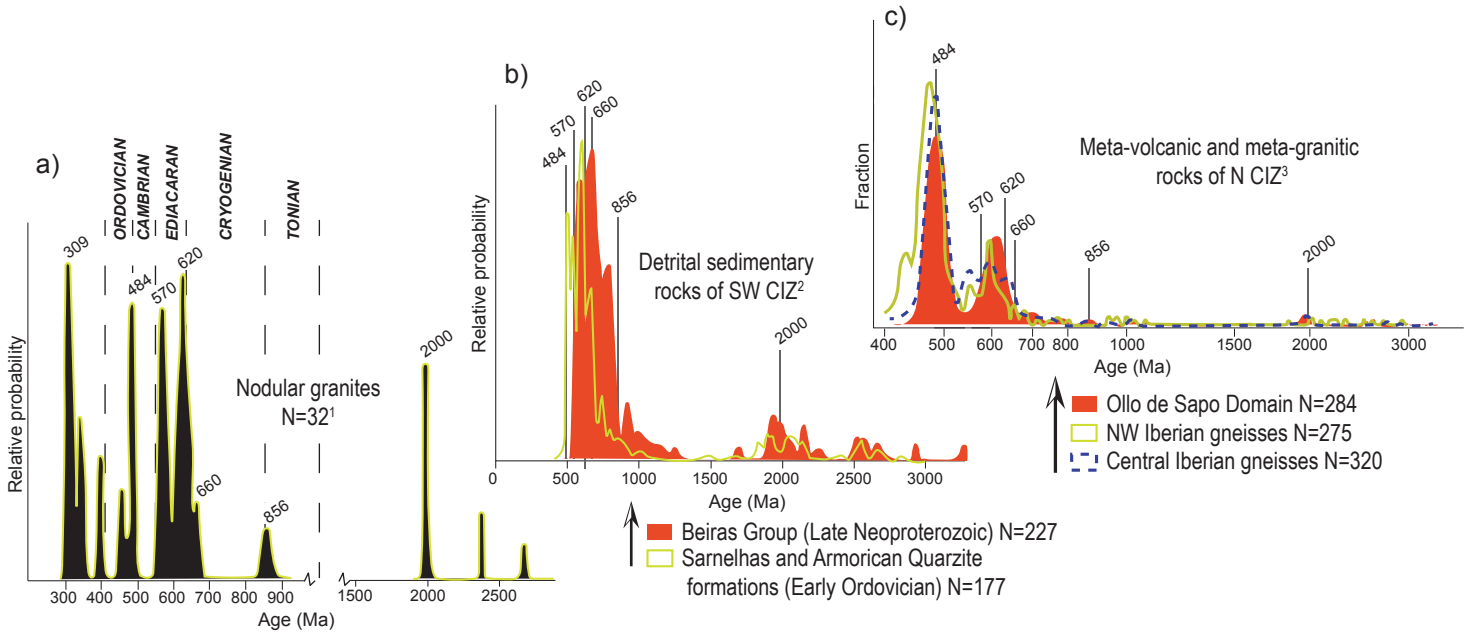

Figure 6. Probability density plots of U-Th-Pb zircon ages obtained from nodular granites (J706-43) and late Neoproterozoic to Ordovician reference domains of the Central Iberian Zone (CIZ). a) Probability distribution of 206Pb/238U ages of nodular granites. 207Pb/206Pb are preferred for ages older than 1 Ga. Main peaks are noted for further comparison. b) Probability plot of detrital zircon ages from late Neoproterozoic greywackes (Beiras Group) and Early Ordovician quartzites (Sarnelhas and Armorican Quarzite formations) of SW CIZ. Grey vertical lines indicate the major probability peaks in the nodular granite sample. c) U-Pb age distribution of metagranites and metavolcanic rocks from Ollo de Sapo Domain and Central Iberian and NW Iberian gneisses of North CIZ. Major peaks observed in the nodular granite sample are included. N: number of analysis.
1: This study; 2: Pereira et al. (2012); 3: Talavera et al. (2013) and references therein.

Figure 7

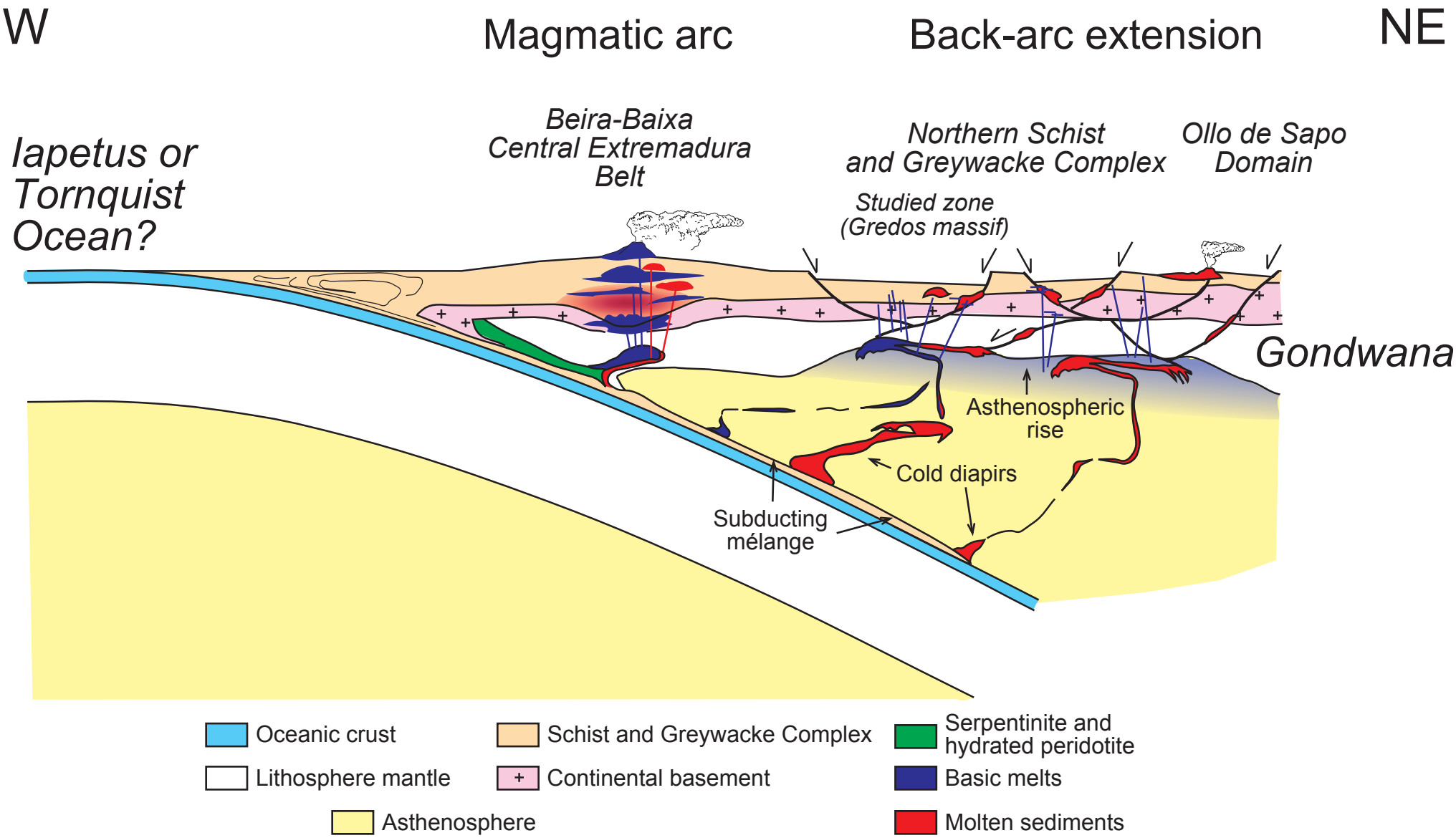

Figure 7. Schematic cross-section (not to scale) depicting a tectonic model for the origin of the Cambro-Ordovician magmatism of the Central Iberian Zone (Iberian Massif). Cold diapirs rooted in the subduction mélange (e.g. Gerya and Yuen, 2003, Castro and Gerya, 2008) ascended through the mantle wedge and accumulated at the basal part of the lithosphere, giving place to partially molten resevoirs of mafic or intermediate to felsic magmas (e.g. Castro and Gerya, 2008, Castro et al., 2010, Hacker et al., 2011) and feeding the magmatic arc and the extensional back-arc region. Cold diapirs made by molten sediments predominated at the back-arc region. The arc-back-arc setting shown in the section is inspired in similar interpretative sketches for this Cambro-Ordovician event published by Fernández et al. (2008), Rubio Ordóñez et al. (2012) and Villaseca et al. (2014).